

MoHETS: Long-term Time Series Forecasting with Mixture-of-Heterogeneous-Experts

Evandro S. Ortigossa¹ Guy Lutsker^{1,2} Eran Segal^{1,3}

Abstract

Real-world multivariate time series can exhibit intricate multi-scale structures, including global trends, local periodicities, and non-stationary regimes, which makes long-horizon forecasting challenging. Although sparse Mixture-of-Experts (MoE) approaches improve scalability and specialization, they typically rely on homogeneous MLP experts that poorly capture the diverse temporal dynamics of time series data. We address these limitations with MoHETS, an encoder-only Transformer that integrates sparse Mixture-of-Heterogeneous-Experts (MoHE) layers. MoHE routes temporal patches to a small subset of expert networks, combining a shared depthwise-convolution expert for sequence-level continuity with routed Fourier-based experts for patch-level periodic structures. MoHETS further improves robustness to non-stationary dynamics by incorporating exogenous information via cross-attention over covariate patch embeddings. Finally, we replace parameter-heavy linear projection heads with a lightweight convolutional patch decoder, improving parameter efficiency, reducing training instability, and allowing a single model to generalize across arbitrary forecast horizons. We validate across seven multivariate benchmarks and multiple horizons, with MoHETS consistently achieving state-of-the-art performance, reducing the average MSE by 12% compared to strong recent baselines, demonstrating effective heterogeneous specialization for long-term forecasting.

1. Introduction

Time series forecasting is a critical task for decision-making in a wide variety of domains such as energy management (Lago et al., 2021), financial planning (Nie et al., 2024), healthcare (Lutsker et al., 2026), and climate analysis (Zhang et al., 2023). However, accurately predicting future values from historical observations is challenging, as real-world time series data often present complex temporal dependencies, seasonality, trends, non-stationarity, and exogenous influences that lead to varied distributions even within short context windows (Wang et al., 2024b; Liu et al., 2024a). Traditional statistical methods, including ARIMA, exponential smoothing, and vector autoregression (Ortigossa et al., 2025), often struggle to capture nonlinear patterns, multiple seasonalities, or high-dimensional multivariate interactions. Furthermore, these challenges intensify in long-term time series forecasting, where predicting intricate cross-variate dependencies over extended contexts demands models that scale efficiently while maintaining predictive accuracy (Liu et al., 2023).

Deep learning approaches have demonstrated remarkable performance in time series forecasting by enabling robust modeling of nonlinear and multivariate patterns. Initially designed for natural language processing (NLP), the Transformer architecture (Vaswani et al., 2017) has been successfully extended to computer vision (CV) (Dosovitskiy et al., 2020), audio (Gong et al., 2021), and time series (Zhou et al., 2021; Wen et al., 2023). Transformer models introduce attention mechanisms that adaptively weight historical information to capture long-range dependencies (Zhou et al., 2021). However, a fundamental misalignment persists in the context of time series: standard Transformers, designed for the discrete semantics of NLP, apply homogeneous processing, typically using dense MLPs, to all tokens. Time series data, conversely, are composed of distinct structural components, persistent periodicities, and transient trends that require fundamentally different inductive biases. Applying a uniform architecture to disentangle these heterogeneous patterns often results in inefficient parameter usage and sub-optimal fittings (Dong et al., 2024).

Recent improvements have pushed Transformers to mitigate these issues. Patching techniques reduce complex-

¹Department of Computer Science and Applied Mathematics, Weizmann Institute of Science, Rehovot, Israel ²Department of Molecular Cell Biology, Weizmann Institute of Science, Rehovot, Israel ³Mohamed bin Zayed University of Artificial Intelligence, Abu Dhabi, UAE. Correspondence to: Eran Segal <eran.segal@weizmann.ac.il>.

ity (Nie et al., 2022), integration of exogenous variables allows learning contextual correlations (Liu et al., 2024c; Wang et al., 2024b), and sparse designs enable more efficient scaling (Shi et al., 2024; Liu et al., 2024a). Although recent sparse approaches have introduced Mixture-of-Experts (MoE) to reduce computational overhead, they essentially inherit the homogeneous expert design of large language models (LLMs), where every expert is an identical MLP (Shi et al., 2024; Liu et al., 2024a). This design ignores the multi-scale nature of time series, where capturing high-frequency local variations requires different operators than modeling long-term global dependencies. To address these challenges, we designed MOHETS, a novel encoder-only Transformer model that integrates sparse Mixture-of-Heterogeneous-Experts (MoHE) with patch-based embedding and covariate integration, improving its robustness to diverse temporal dependencies and patterns. We demonstrate that MOHETS consistently outperforms well-known state-of-the-art models in forecasting benchmark experiments. In summary, the main contributions of this research are as follows:

- We introduce MOHETS, an encoder-only Transformer with a Mixture-of-Heterogeneous-Experts (MoHE) strategy that applies architecturally distinct experts to effectively model time patterns at different levels, ensuring the model architecture aligns with the intrinsic decomposition of time-series data.
- We incorporate a multimodal cross-attention module that integrates external information from exogenous covariates. With this design, MOHETS enhances time series representations by capturing interactions between endogenous features and exogenous information.
- We propose the MoHE layer, which combines depth-wise convolutions and Fourier-based experts to capture global trends and local periodicities at the patch level, respectively, enhancing specialization while maintaining the scaling benefits of standard MoEs.

2. Related Work

2.1. Deep Learning for Time Series Forecasting

Deep learning models have significantly advanced time series forecasting, transitioning from MLP-based networks (Wang et al., 2024a), recurrent neural networks (RNNs) (Salinas et al., 2020), and convolutional neural networks (CNNs) (Sen et al., 2019) to Transformer-based architectures (Wen et al., 2023). The attention mechanism of Transformers is able to adaptively weight historical information, making it a natural choice for handling long-term dependencies. Early Transformer models, such as Informer (Zhou et al., 2021), introduced the ProbSparse self-attention to address the quadratic complexity of stan-

dard Transformers, while Autoformer (Wu et al., 2021b) leveraged auto-correlation to discover period-based dependencies at the subseries level. Recently, PatchTST (Nie et al., 2022) further improved efficiency by applying channel-independent processing and segmenting time series into subseries-level patches, reducing computational overhead while preserving local semantics and allowing the model to attend longer context windows. iTransformer (Liu et al., 2023) inverts the input dimensions to apply attention across variates rather than time, prioritizing multivariate correlations over temporal dependencies. Foundation models, such as TimeGPT (Garza et al., 2023) and TimesFM (Das et al., 2024), explore pre-training paradigms to improve adaptability. However, these architectures are predominantly dense and homogeneous. By processing diverse temporal dynamics, such as high-frequency noise and low-frequency trends, through identical operators (e.g., standard MLPs), they suffer from parameter redundancy and struggle to decouple entangled temporal patterns.

2.2. Forecasting with Covariates

Real-world time series are often partially observed, and endogenous variables (the primary series to forecast) are frequently influenced by exogenous covariates, which capture external contexts that can affect temporal dynamics and consequently predictions (Wang et al., 2024b). Covariates encompass external contexts such as calendar events, weather metrics, or economic indicators that drive the non-stationary dynamics of the target series. Transformer-based models have increasingly introduced covariates to improve contextual understanding. The Temporal Fusion Transformer (TFT) (Lim et al., 2021) employed variable selection networks and entity embeddings to dynamically weigh covariates, while Timer-XL (Liu et al., 2024b) supports covariate-informed forecasting in a decoder-only patched architecture. Incorporating such data requires careful handling to address issues such as missing values or temporal misalignment. In this context, TimeXer (Wang et al., 2024b) refined covariate incorporation by implementing a patch-wise self-attention module for endogenous series and a variate-wise cross-attention module for exogenous inputs, thus mitigating issues related to partial observability and temporal misalignment. Exogenous covariates can provide valuable external information to enhance robustness to non-stationarity and improve forecasting accuracy. However, current methods often append covariates as auxiliary tokens or simplified concatenations (Lim et al., 2021; Das et al., 2023), failing to explicitly model the cross-modal interaction between static external contexts and dynamic time patches.

2.3. Sparse Mixture-of-Experts (MoE)

Deep learning models are dense, imposing high memory and computational costs during training and inference (Shi

et al., 2024). Sparse architectures, such as Mixture-of-Experts (MoE), dynamically route inputs to specialized sub-networks for conditional activation, enabling scaling up the model’s capacities while reducing computational overhead (Shazeer et al., 2017; Fedus et al., 2022). Model sparsification has received considerable attention in the context of NLP and CV for efficient handling of diverse patterns (Fedus et al., 2022; Jiang et al., 2024; Dai et al., 2024; Riquelme et al., 2021), but has received relatively less attention in time-series research, with few relevant works implementing such an approach (Shi et al., 2024). While MoLE (Ni et al., 2024) explores linear ensembling, recent works like Time-MoE (Shi et al., 2024) and Moirai-MoE (Liu et al., 2024a) adapt sparse MoE to decoder-only Transformers. However, these models strictly adhere to the NLP-standard and rely on MLP-based expert designs. Training stability and expert specialization are challenges when applying MoE, as routing mechanisms can lead to load imbalance or overfitting (Fedus et al., 2022). Crucially, the direct adaptation of NLP-centric MoEs overlooks the signal processing nature of time series. Standard MLP experts lack the inductive bias to efficiently separate global trends from local periodicities (Dong et al., 2024), a task for which specialized operators such as Convolutions and Fourier Transforms have been mathematically shown to outperform MLPs (Wang et al., 2024a).

We bridge this gap with MOHETS, replacing homogeneous MLPs with a Mixture-of-Heterogeneous-Experts that assigns architecturally distinct operators to the specific temporal components they are best suited to model.

3. Methodology

Problem Statement. Let $\mathbf{X} \in \mathbb{R}^{D \times T}$ denote a set of multivariate time series with D variates (or channels) and T time steps, where each $\mathbf{x}_t = [x_t^1, x_t^2, \dots, x_t^D]^\top \in \mathbb{R}^D$ represents the observations across all variates at time t . Given a look-back window of length L , the objective is to estimate the next H time steps (the forecast horizon), which yields the forecast of $\hat{\mathbf{X}}_{T+1:T+H} \in \mathbb{R}^{D \times H}$, conditioned on the historical sequence $\mathbf{X}_{T-L+1:T} \in \mathbb{R}^{D \times L}$. The input sequence is processed by a learnable embedding module and projected to the latent dimension d_{model} (detailed in Section 3.2) Next, the input embeddings are forwarded to the Transformer backbone. A typical Transformer model is constructed by stacking B Transformer blocks, where each block can be represented as follows:

$$\mathbf{u}_t^b = \text{Attn}(\text{Norm}(\mathbf{h}_t^{b-1})) + \mathbf{h}_t^{b-1}, \quad (1)$$

$$\mathbf{h}_t^b = \text{FFN}(\text{Norm}(\mathbf{u}_t^b)) + \mathbf{u}_t^b, \quad (2)$$

where $\text{Attn}(\cdot)$ denotes the self-attention module, $\text{Norm}(\cdot)$ are normalization modules, $\text{FFN}(\cdot)$ denotes the Feed-Forward Network, and $b \in \{0, \dots, B-1\}$ denotes the b -th Transformer block (Vaswani et al., 2017). Standard

Transformers rely on dense computations, where a single shared FFN processes every token, effectively forcing a “one-size-fits-all” transformation. In contrast, sparse MoE layers enable conditional computation. To introduce sparsity and enable parameter scaling while keeping computational costs, an emerging practice is to replace FFN modules in a Transformer with MoE layers. An MoE layer consists of several sparsely activated expert networks, where each expert is structurally identical to a standard FFN (Shi et al., 2024; Dai et al., 2024). Then, each individual time point can be routed through a gating mechanism to one or more selected experts (Fedus et al., 2022; Lepikhin et al., 2021) as follows:

$$\mathbf{h}_t^b = \text{MoE}(\text{Norm}(\mathbf{u}_t^b)) + \mathbf{u}_t^b, \quad (3)$$

with

$$\text{MoE}(\text{Norm}(\mathbf{u}_t^b)) = \sum_{i=1}^N (g_{i,t} \text{FFN}_i(\text{Norm}(\mathbf{u}_t^b))), \quad (4)$$

$$g_{i,t} = \begin{cases} s_{i,t}, & s_{i,t} \in \text{Topk}(\{s_{j,t} | 1 \leq j \leq N\}, K), \\ 0, & \text{otherwise,} \end{cases} \quad (5)$$

$$s_{i,t} = \text{Softmax}_i(\mathbf{W}_i^b(\text{Norm}(\mathbf{u}_t^b))), \quad (6)$$

where N represents the number of FFN experts, $g_{i,t}$ is the gate value for the i -th expert, $\text{Topk}(\cdot, K)$ is the set of K highest affinity scores between the t -th time point and all experts, $s_{i,t}$ is the point-to-expert affinity score computed by taking the Softmax logits from the gate function $\mathbf{W}_i^b \in \mathbb{R}^{d_{\text{model}} \times N}$, a learnable linear projection (Shazeer et al., 2017). Therefore, each time point will be forwarded only to K of the N experts, allowing the activated experts to specialize in different time patterns and ensuring computational efficiency (Liu et al., 2024a; Dai et al., 2024).

3.1. MoHETS Architecture

Our proposed MOHETS, illustrated in Figure 1, adopts an encoder-only Transformer backbone that leverages recent advances in stability optimizations from large-scale language models (Grattafiori et al., 2024; Dai et al., 2024). Specifically, we employ RMSNorm (Zhang & Sennrich, 2019) in the Norm modules to normalize inputs to each Transformer sub-layer, enhancing training stability (Xiong et al., 2020). In forecasting, the relative distance between time steps (e.g., “24 hours ago”) carries more predictive signal than absolute indices (Erturk et al., 2025). Consequently, we replace standard additive positional encodings with Rotary Position Embeddings (RoPE) (Su et al., 2024). By injecting position information directly into the attention query-key products, RoPE improves the model’s ability to extrapolate to unseen future horizons. Finally, to structurally decouple the modeling of global trends and local periodicities, we replace dense FFNs with our MoHE lay-

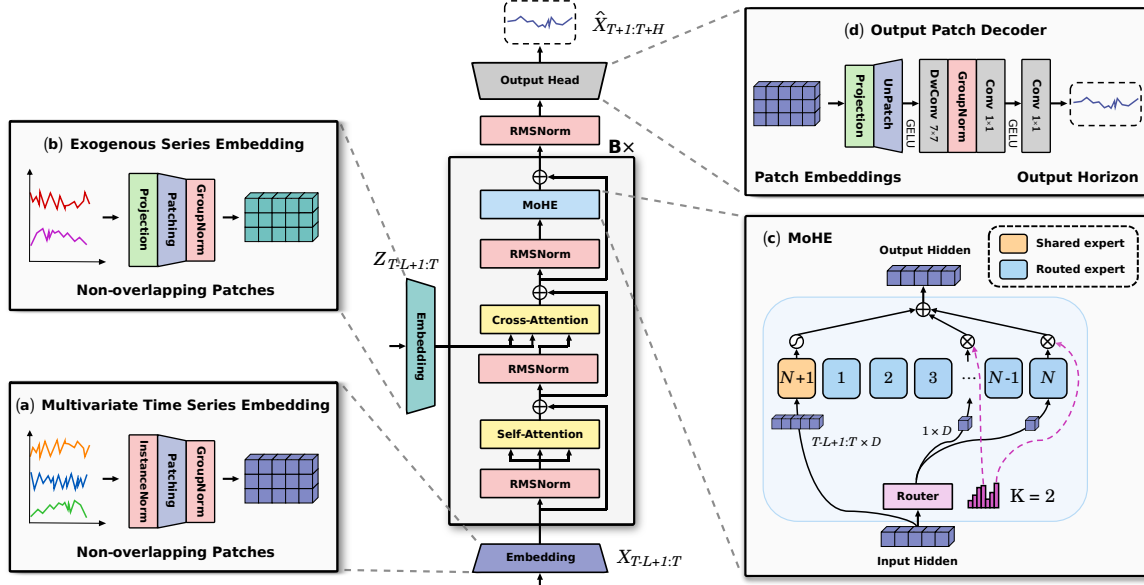


Figure 1. Architecture of MoHETS, an encoder-only transformer for multivariate time-series forecasting. (a) The input embedding module splits time channels into sequences of channel-independent patch embeddings. (b) The exogenous embedding module projects, fuses, and patches covariates with the input series to produce aligned exogenous patch embeddings. These patches are processed through B stacked Transformer blocks; each block is composed of self-attention, cross-attention, and a (c) Mixture-of-Heterogeneous-Experts (MoHE), where a shared depthwise-convolution expert maintains sequence continuity and routed Fourier experts resolve local spectral patterns. (d) The patch decoder head projects final embeddings to forecasting horizons.

ers. This design enables conditional computation by dynamically routing patches to the operators best suited to their signal characteristics.

3.2. Input Embedding

To mitigate distribution shift issues in non-stationary time series, we apply instance normalization to the input sequence (Liu et al., 2022b), which normalizes each input variate by its instance mean and variance before patching and denormalizes the output predictions to restore the original scale. Standard Transformers process time series sequences as time-point tokens, with quadratic complexity in the look-back length L . To address this limitation, patching techniques segment the input sequence into subseries (Nie et al., 2022), treating each patch as a semantic token (Liu et al., 2024a). Specifically, for a patch length P , the look-back window $\mathbf{X}_{T-L+1:T}$ is embedded into $S = \lceil L/P \rceil$ non-overlapping patches $\mathbf{P} = \{\mathbf{p}_1, \mathbf{p}_2, \dots, \mathbf{p}_S\}$, $\mathbf{p}_i \in \mathbb{R}^{D \times P}$, effectively decreasing the quadratic attention complexity to $O(S^2)$ while aggregating high-frequency local noise into robust feature vectors. Our patch embedding process is illustrated in Figure 1a and defined as:

$$\begin{aligned} \{\mathbf{p}_1, \mathbf{p}_2, \dots, \mathbf{p}_S\} &= \text{Patchify}(\mathbf{x}), \\ \mathbf{h}_p^0 &= \text{PatchEmbed}(\text{GNorm}(\mathbf{p})), \end{aligned} \quad (7)$$

where $\mathbf{h}_p^0 \in \mathbb{R}^{d_{\text{model}}}$ is the embedded representation of patch \mathbf{p}_i and GNorm applies a single-group normalization to the

embedding dimension (Wu & He, 2018). Furthermore, the channel independence approach (Nie et al., 2022) is used to process each variate of a multivariate input as a univariate series, allowing MoHETS to operate in any-variate forecasting tasks.

3.3. Self-Attention

To capture temporal dependencies across patch embeddings, we implement multi-head self-attention (see Equation 1) optimized for efficiency and extrapolation. To efficiently handle extended look-back windows (L), we employ FlashAttention-2 (Dao, 2023). This implementation reformulates the scaled dot-product to reduce memory access costs from quadratic to linear with respect to sequence length, enabling rapid training on long sequences. We further reduce the inference memory footprint by implementing grouped-query attention (GQA) (Ainslie et al., 2023). By sharing a single key-value head across multiple query heads, GQA maintains the expressivity of multi-head attention while significantly reducing the memory overhead needed for autoregressive rollout. Following Shi et al. (2024), we adopt a bias-free architecture for all layers except the QKV projections. Retaining QKV biases has been shown to preserve length extrapolation capabilities by maintaining shift-invariance in the attention scores (Chowdhery et al., 2023). In addition, we apply channel-independent attention per variate (Nie et al., 2022). This mechanism forces the model to learn universal temporal dynamics (e.g., seasonality) that

generalize across different variates, preventing overfitting to spurious cross-variate correlations. Details about our implementation of multi-head attention are in Appendix A.5.

3.4. Multimodal Cross-Attention

Let $\mathbf{Z}_{T-L+1:T+H} \in \mathbb{R}^{C \times (L+H)}$ denote an additional sequence with C covariate dimensions, such as calendar indicators or weather metrics, assumed to be known over the forecast horizon (Wang et al., 2024b). We design a multimodal embedding module that incorporates exogenous covariate information into endogenous time series. The module operates in two stages. First, we use linear layers to project both endogenous and covariate sequences to the model dimension d_{model} :

$$\begin{aligned}\mathbf{W}_t^X &= \text{Linear}_X(\mathbf{x}_t), \quad \mathbf{x}_t \in \mathbb{R}^D, \quad \mathbf{W}_t^X \in \mathbb{R}^{d_{\text{model}}}, \\ \mathbf{W}_t^Z &= \text{Linear}_Z(\mathbf{z}_t), \quad \mathbf{z}_t \in \mathbb{R}^C, \quad \mathbf{W}_t^Z \in \mathbb{R}^{d_{\text{model}}},\end{aligned}\quad (8)$$

These projections are fused via concatenation and a subsequent projection layer: $\mathbf{w}_t^M = \text{Linear}_{\text{fuse}}([\mathbf{w}_t^X; \mathbf{w}_t^Z])$, creating a covariate-enriched latent representation aligned with the endogenous dimension D . Concatenation followed by linear projection outperforms alternatives such as element-wise addition or direct concatenation (Bao et al., 2023). As illustrated in Figure 1b, the fused sequence $\mathbf{W}_t^M \in \mathbb{R}^{D \times L}$ is then patched and embedded into $S = \lceil L/P \rceil$ non-overlapping tokens, serving as keys and values for the cross-attention mechanism. By adopting this approach, we ensure that exogenous information is aggregated into endogenous data regardless of the difference between D and C .

In the cross-attention module, the self-attention output (Section 3.3) serves as the query, while the multimodal patch embeddings feed the key and value projections (Wang et al., 2024b). This design allows the model to dynamically retrieve external context such as “holiday effects” or “weather spikes”, conditional on the current state. Cross-attention enables a Transformer model to combine information from different modalities, acting as a connector between representations from one modality by attending to another. Our cross-attention module computes multi-head attention with optimizations that mirror those of the self-attention module (Section 3.3), specifically FlashAttention (Dao, 2023) for efficient scaled dot-product computation and GQA (Ainslie et al., 2023) to reduce memory overhead by clustering queries and sharing key-value pairs. The above process can be formalized as

$$\mathbf{v}_p^b = \text{CrossAttn}(\text{RMSNorm}(\mathbf{u}_p^b), \mathbf{h}_m) + \mathbf{u}_p^b. \quad (9)$$

Channel independence is maintained through variate-wise processing, ensuring alignment with the endogenous pipeline and scalable covariate integration. Since covariates \mathbf{Z} are known for the future horizon $t = T+1, \dots, T+H$, this fusion process is repeated during the autoregressive rollout,

allowing the model to anticipate future external temporal information before it appears in the series.

3.5. Mixture-of-Heterogeneous-Experts (MoHE)

To enhance specialization and scalability in our Transformer forecaster, we follow recent advances in time series models and replace dense FFNs with sparse MoE layers (Shi et al., 2024). However, standard MoEs are based on homogeneous MLP experts, assuming that all tokens require the same processing logic. We argue that this approach is suboptimal for time series, which are a superposition of global trends and local frequencies. We therefore propose the Mixture-of-Heterogeneous-Experts (MoHE) design based on a structural labor partitioning: assigning sequence-continuity modeling to a shared expert and local-frequency analysis to routed experts. Combining routed experts working at the unit level with a shared expert, which is always activated and operates at the sequence level to capture and consolidate common knowledge, improves specialization robustness (Dai et al., 2024; Shi et al., 2024).

Each MoHE expert, shared or routed, comprises two layers that project time patches from the model dimension d_{model} to an intermediate dimension d_{ff} and back to d_{model} , with a factor of $d_{\text{ff}} = 2 \times d_{\text{model}}$, GELU activation (Hendrycks & Gimbel, 2016), and dropout (Srivastava et al., 2014). The shared expert is a depthwise separable convolution (DwConvFFN) that acts as a time-domain expert: it slides along the sequence dimension to capture continuous trends and maintain temporal coherence across patches. Conversely, the routed experts are Fourier-based networks (FA-FFN) acting as frequency-domain experts. By operating in the spectral domain, FA-FFNs isolate high-frequency periodicities within individual patches – a task where standard MLPs often struggle due to spectral bias (Dong et al., 2024). Specifically, a FA-FFN replaces general-purpose linear layers with FAN modules (Dong et al., 2024), which are designed to leverage the strengths of Fourier series transformations to model periodic patterns from time series signals.

Therefore, a MoHE layer combines one DwConvFFN shared expert and N FA-FFN routed experts:

$$\begin{aligned}\bar{\mathbf{v}}_p^b &= \text{RMSNorm}(\mathbf{v}_p^b), \\ \text{MoHE}(\bar{\mathbf{v}}_p^b) &= g_{N+1,p} \text{DwConvFFN}_{N+1}(\bar{\mathbf{v}}_p^b) \\ &\quad + \sum_{i=1}^N (g_{i,p} \text{FA-FFN}_i(\bar{\mathbf{v}}_p^b)),\end{aligned}\quad (10)$$

where $g_{N+1,p}$ denotes a Sigmoid function gate, modulating the shared expert contribution (Shi et al., 2024), and $g_{i,p}$ represents the router gate value defined in Equation 5 (dotted lines in Figure 1c).

The heterogeneity introduced by the MoHE design draws inspiration from the trend-seasonality decomposition often

used in statistical forecasting (Wu et al., 2021b). However, instead of hard-coding the decomposition, MoHE learns to dynamically route signal components: directing transient noise and short-term periodicity to Fourier experts while reserving the shared convolutional path for persistent sequence-level trends. Sparse architectures dynamically activate different experts to handle heterogeneous data patterns, with each expert specializing in learning different knowledge (Shi et al., 2024). This MoHE design improves specialization over homogeneous MoEs, thereby enhancing generalization and forecasting accuracy for heterogeneous temporal patterns.

3.6. Output Patch Decoder

To map the Transformer’s output from patches to forecast time points, most of the state-of-the-art time series models have implemented linear-based projection heads (Nie et al., 2022; Liu et al., 2023; Wang et al., 2024b; Shi et al., 2024). Standard linear heads flatten the patch embeddings, destroying the local temporal structure preserved by the encoder. Furthermore, the parameter count of a linear head scales as $O(L \times D)$, leading to parameter explosion and overfitting when the number of variates D increases. We replace linear projections with a convolutional patch decoder module (see Figure 1d) that projects the latent dimension d_{model} to time points using a lightweight sequence of convolutions (Liu et al., 2022c). This design imposes a locality inductive bias, ensuring that the output generation relies on the semantic vectors of each patch rather than a global dense matrix, stabilizing training.

Each variate is processed independently by our output patch decoder, maintaining channel independence to handle any-variate forecasting. With this convolutional patch decoder, we provide a lightweight module that mitigates the instability of heavy linear heads, helping MOHETS to achieve superior accuracy in forecasting tasks. Refer to Appendix A.5 for technical details.

3.7. Loss Functions

Time series data often contain transient outliers and extreme spikes that can destabilize training (Wen et al., 2019), especially for sparse models where gradients are routed to specific experts (Fedus et al., 2022). Standard MSE amplifies these outliers quadratically. Therefore, we adopt the Huber loss (Huber, 1992) as our main prediction loss ($\mathcal{L}_{\text{pred}}$), which behaves quadratically for small errors and linearly for large errors, providing a robust gradient signal that prevents expert collapse due to outlier-driven gradients.

However, focusing only on prediction error optimization often leads to stability and convergence challenges due to load imbalance issues when using MoE architectures. Specifically, the sparse gating mechanism introduces the risk of

routing collapse (Shazeer et al., 2017), in which the model converges to a trivial state by selecting a single expert, limiting the opportunities for other experts to receive sufficient training (Dai et al., 2024). To prevent routing collapse, we impose an auxiliary load balancing loss (\mathcal{L}_{aux}) to balance expert utilization (Lepikhin et al., 2021; Fedus et al., 2022; Shi et al., 2024). This loss minimizes the coefficient of variation of the expert assignment probabilities, ensuring a more uniform distribution of tokens across the experts’ pool. We detail the prediction and balance losses in Appendix A.5.

3.8. Training Objective and Forecasting

The training objective combines the prediction loss with the auxiliary balance loss to compose the final loss, ensuring both accuracy and expert balance:

$$\mathcal{L} = \mathcal{L}_{\text{pred}} \left(\mathbf{X}_{T+1:T+H_o}, \hat{\mathbf{X}}_{T+1:T+H_o} \right) + \alpha \mathcal{L}_{\text{aux}}, \quad (11)$$

where H_o is the length of the predicted future time steps and α is the expert balance factor. The patch length is uniformly set as P from the input embedding to the output patch decoder, with MOHETS supporting flexible output resolutions H_o .

Time series models have been trained with different look-back lengths, ranging from small (Wang et al., 2024b) to large values (Shi et al., 2024). Very small look-back windows lack contextual information critical for long-term forecasting, while very long windows can introduce undesirable noise. We standardize the look-back window to $L = 672$ (approximately 4 weeks of hourly data). This duration balances the need to capture monthly seasonality with the computational cost of attention, avoiding the diminishing returns often observed with ultra-long contexts in noisy real-world data (Liu et al., 2024c). MOHETS is trained as a one-for-all forecaster (Liu et al., 2024b). During inference, we employ autoregressive rolling forecasting: the model predicts a fixed chunk (H_o next steps), which is appended to the input buffer to predict the subsequent chunk. This approach allows a single trained model to generate arbitrary horizons (e.g., $\{96, 192, 336, 720\}$) without retraining for any specific length.

3.9. Model Settings and Training Details

MOHETS and all experiments are implemented in PyTorch (Paszke et al., 2019). Trainings are performed on a single NVIDIA A100 (80GB) GPU. To maximize throughput without sacrificing numerical stability, we utilized TensorFloat-32 (TF32) precision, which provides the dynamic range of FP32 with the matrix-multiplication speed of FP16. We experiment with the number of Transformer blocks searched from $B \in \{4, 6, 8\}$, the dimension of representations d_{model} from $\{64, 128, 256, 384\}$, the patch length as $P \in \{8, 12, 16\}$, and the output resolution as

$H_o \in \{16, 24, 32\}$ time points. Following the results achieved by (Dai et al., 2024; Liu et al., 2024a; Shi et al., 2024), we set 8 as the number of experts per MoHE layer with $K = 2$, which is an optimal choice to balance performance and computational efficiency (Shi et al., 2024).

For optimization, we apply the fused implementation of AdamW (Loshchilov & Hutter, 2017) with a maximum learning rate of 3.2×10^{-3} , $\text{weight_decay} = 1 \times 10^{-4}$, $\beta_1 = 0.9$, and $\beta_2 = 0.95$ (Chen et al., 2020). Furthermore, we use a Cosine Annealing scheduler with a linear warmup (Loshchilov & Hutter, 2016) for the first 10% training steps, and a decay to a minimum learning rate of 1.2×10^{-4} and early stopping with $\text{patience} = 5$. Such an aggressive warmup is essential to stabilize the router's initial random assignment before the experts begin specializing. Following (Shi et al., 2024), we set the Huber loss δ to 2.0 and the auxiliary loss factor α to 0.02. Training epochs are searched from 10 to 30. We do not use data augmentations. Refer to Appendix A.4 for more optimization details.

4. Main Results

We conduct extensive experiments to evaluate the performance and efficiency of MoHETS in long-term multivariate forecasting tasks. Our experiments include 7 benchmark datasets that cover a wide variety of real-world domains with different temporal resolutions and number of variables, as well as 15 baseline models representing the state-of-the-art in long-term forecasting. A detailed summary of each benchmark data is provided in Appendix A.1 while the baseline models are presented in Appendix A.2. As evaluation metrics, we adopt the mean squared error (MSE) and the mean absolute error (MAE), detailed in Appendix A.3.

To ensure fair comparisons, we follow the data processing and train-validation-test split protocol defined by (Wu et al., 2023), where the train, validation, and test datasets are split chronologically to prevent data leakage. Each benchmark is performed over four long-term prediction horizons, which are $H \in \{96, 192, 336, 720\}$. Furthermore, we feed the cross-attention modules of MoHETS only with calendar information derived from the timestamp of each instance, splitting the calendar components and scaling them to continuous linear frequency values (Alexandrov et al., 2020).

4.1. Multivariate Time Series Forecasting

Table 1 shows long-term multivariate forecasting results. MoHETS establishes a new state-of-the-art, surpassing the strongest baseline (TimeXer, SOFTS) on all datasets. In particular, it dominates on datasets with strong seasonality (ETTh1, ETTm2), validating the MoHE architecture's ability to decouple periodic patterns. When analyzing each average performance over the horizons $\{96, 192, 336, 720\}$,

MoHETS reduces the average MSE by 12.3% relative to TimeXer on the ETTh1 dataset, by 10% relative to TimeMixer on Weather, and by 5.1% relative to SOFTS on the Traffic data, demonstrating the efficacy of its MoHE architecture and support for covariate injection. The complete results and comparisons with time series foundation models are included in Appendix B.

4.2. Ablation Study

We validate the effectiveness of our designs in MoHETS by conducting detailed ablation studies on key architectural components using experimental benchmarks, including the Transformer backbone type, various compositions of our MoHE approach, the incorporation of exogenous covariates, normalization, and the final projection head. We fix $d_{\text{model}} = 128$ (see Section 3.9) and limit the maximum number of training epochs to 20 in each ablation experiment to save computational time. All results are averaged over the horizons $H \in \{96, 192, 336, 720\}$, with lower MSE or MAE values indicating better performance.

Transformer Backbone Type. We compare MoHETS with encoder-only and decoder-only backbones. Table 2 shows that the encoder-only design outperforms the decoder-only variant, achieving average MSE reductions of 8.1% on ETTh1 and 9.6% on Traffic. Additionally, the encoder-only approach is more flexible in supporting longer output resolutions, which can help mitigate the accumulation of autoregressive errors in long-horizon forecasting.

MoHE Configurations. Once the encoder-only architecture is established as our default backbone, we ablate different expert compositions for the MoHE layers: all MLP-FFNs (i.e., a standard MoE as defined in Equation 4), all FA-FFNs, mixing a DwConvFFN with MLP-FFNs, and mixing a simple ConvFFN, composed of two pointwise convolution layers, with MLP-FFNs or FA-FFNs. Table 3 shows that our proposed mixture (DwConvFFN + FA-FFNs) achieves improvements in average MSE of 4.0% on ETTh1 and 18.5% on Traffic over the all-MLP version. These results validate our hypothesis on the complementary expertise of the Mixture-of-Heterogeneous-Experts approach, specifically replacing traditional MLP-FFN experts with Fourier-based networks.

Normalization Strategies. We evaluate different normalization strategies, including homogeneous approaches with LayerNorm (Ba et al., 2016) or RMSNorm throughout the model (standard approach), and a mixed approach with a single-group group normalization (equivalent to a LayerNorm on channel dimensions) in the input patching and output projection, RMSNorm elsewhere (our proposal), inspired by CvT (Wu et al., 2021a). Table 4 shows that the mixed approach achieves significantly lower MSE and

Table 1. Results of long-term multivariate forecasting experiments. Full-shot results are obtained from (Liu et al., 2023; Wang et al., 2024b; Han et al., 2024). **Bold red**: the best, underlined blue: the second best. Results are averaged from all prediction horizons $H = \{96, 192, 336, 720\}$. 1st Count represents the number of wins achieved by a model.

Models	MoHETS		SOFTS		TimeXer		iTransformer		TimeMixer		TimesNet		PatchTST		Crossformer		TiDE		DLinear		FEDformer	
Metrics ↓	MSE	MAE	MSE	MAE	MSE	MAE	MSE	MAE	MSE	MAE	MSE	MAE	MSE	MAE	MSE	MAE	MSE	MAE	MSE	MAE	MSE	MAE
ETTh1	0.383	0.412	0.449	0.442	<u>0.437</u>	<u>0.437</u>	0.454	0.447	0.448	0.442	0.454	0.450	0.469	0.454	0.529	0.522	0.540	0.507	0.455	0.451	0.440	0.459
ETTh2	0.348	0.382	0.373	0.400	0.367	0.396	0.383	0.406	<u>0.364</u>	<u>0.395</u>	0.414	0.496	0.387	0.407	0.942	0.683	0.611	0.549	0.558	0.515	0.436	0.449
ETTm1	0.333	0.367	0.393	0.403	0.382	0.397	0.407	0.410	<u>0.381</u>	<u>0.395</u>	0.400	0.405	0.387	0.400	0.513	0.495	0.419	0.419	0.403	0.406	0.448	0.452
ETTm2	0.256	0.310	0.287	0.330	<u>0.274</u>	<u>0.322</u>	0.288	0.332	0.275	0.323	0.291	0.332	0.281	0.326	0.757	0.610	0.358	0.403	0.350	0.400	0.304	0.349
Weather	0.216	0.249	0.255	0.278	0.241	<u>0.271</u>	0.258	0.278	<u>0.240</u>	<u>0.271</u>	0.259	0.286	0.259	0.281	0.258	0.315	0.270	0.320	0.265	0.316	0.308	0.360
ECL	0.158	0.251	0.174	<u>0.264</u>	<u>0.171</u>	0.270	0.178	0.270	0.182	0.272	0.192	0.295	0.205	0.290	0.244	0.334	0.251	0.344	0.212	0.300	0.214	0.327
Traffic	0.388	0.256	<u>0.409</u>	<u>0.267</u>	0.466	0.287	0.428	0.282	0.484	0.297	0.620	0.336	0.481	0.304	0.550	0.304	0.760	0.473	0.625	0.383	0.609	0.376
Average	0.297	0.318	<u>0.334</u>	0.341	<u>0.334</u>	<u>0.340</u>	0.342	0.346	0.339	0.342	0.376	0.371	0.353	0.352	0.542	0.466	0.458	0.431	0.410	0.396	0.394	0.396
1 st Count	16	0	0	0	0	0	0	0	0	0	0	0	0	0	0	0	0	0	0	0	0	0

Table 2. Ablation study with different Transformer types. The best results are in **bold**.

Dataset	ETTh1		ETTh2		ETTm1		ETTm2		Weather		ECL		Traffic	
	MSE	MAE	MSE	MAE	MSE	MAE	MSE	MAE	MSE	MAE	MSE	MAE	MSE	MAE
Encoder	0.383	0.415	0.362	0.389	0.338	0.366	0.270	<u>0.313</u>	0.244	<u>0.265</u>	0.164	0.254	0.406	0.276
Decoder	0.417	0.430	0.371	0.395	0.354	0.375	0.269	0.315	0.255	0.270	0.167	0.262	0.449	0.297

Table 3. Ablation study with different expert architectures. The best results are in **bold** and the second best are underlined.

Dataset	ETTh1		ETTh2		ETTm1		ETTm2		Weather		ECL		Traffic	
	MSE	MAE												
MoHETS	0.383	0.415	0.362	<u>0.389</u>	0.338	0.366	0.270	<u>0.313</u>	0.244	<u>0.265</u>	0.164	0.254	0.406	0.276
MLP	0.399	0.420	<u>0.361</u>	0.392	0.348	0.373	<u>0.264</u>	0.314	0.262	0.272	0.267	0.318	0.498	0.331
FA	<u>0.391</u>	0.421	0.364	<u>0.390</u>	0.352	0.377	0.268	0.314	0.230	0.262	<u>0.174</u>	0.269	0.428	0.290
Conv + MLP	0.398	<u>0.420</u>	0.357	0.389	0.353	0.378	0.260	0.312	<u>0.234</u>	<u>0.265</u>	0.197	0.293	0.435	0.284
Conv + FA	0.402	0.425	0.367	0.395	0.356	0.376	0.269	<u>0.312</u>	0.237	0.266	0.164	<u>0.255</u>	0.413	0.276
DwConv + MLP	0.401	0.424	0.372	0.404	0.368	0.375	0.279	0.325	0.368	0.283	0.239	0.325	0.420	0.284

Table 4. Ablation study using different normalization layers, projection head, and with no covariate injection. The best results are in **bold** and the second best are underlined.

Dataset	ETTh1		ETTh2		ETTm1		ETTm2		Weather		ECL		Traffic	
	MSE	MAE												
MoHETS	0.383	0.415	<u>0.362</u>	<u>0.389</u>	0.338	0.366	<u>0.270</u>	<u>0.313</u>	0.244	<u>0.265</u>	0.164	0.254	0.406	0.276
LayerNorm	0.425	0.437	0.458	0.442	0.362	0.379	0.280	0.326	0.281	0.284	0.164	<u>0.256</u>	0.413	0.270
RMSNorm	0.436	0.444	0.439	0.436	0.358	0.377	0.278	0.322	0.229	0.259	0.188	0.274	0.430	0.288
MLP-based head	0.457	0.451	<u>0.354</u>	<u>0.392</u>	<u>0.351</u>	0.380	0.259	0.314	0.237	0.272	0.177	0.276	0.418	0.301
w/o exogenous covs.	<u>0.418</u>	<u>0.429</u>	0.381	0.398	0.357	<u>0.375</u>	0.283	0.323	0.247	0.269	<u>0.174</u>	0.264	0.409	0.273

MAE values than homogeneous normalizations on most benchmarks, with 9.9% and 12.1% improvements in MSE over all-LayerNorm and all-RMSNorm, respectively, on ETTh1. However, the all-RMSNorm version presents a strong MSE on the Weather dataset.

Projection Heads. We compare the convolutional output decoder with traditional MLP-based heads. The convolutional design outperforms the MLP-based head by reasonable margins in most tests (Table 4), validating that the convolutional locality’s inductive bias is superior to dense linear projections for decoding. By respecting the patch boundary structure during upsampling, the convolutional head prevents overfitting on the output layer.

Exogenous Covariates. Incorporating covariates through our multimodal cross-attention approach improves performance (Table 4), particularly on datasets with lower dimensionality such as ETT. RoPE provides relative positions, but it lacks semantic context. A positional embedding informs the model that a time point t is after $t - 1$, but not that t corresponds to a “holiday,” for example. Our cross-attention mechanism injects this semantic awareness directly, critical for modeling non-stationary shifts driven by human calendars. We observe a slight reduction in the advantage of injecting calendar information as data dimensionality increases, as in Traffic. Note that we only experimented with calendar information as covariates, which significantly improved robustness to non-stationarity in coarse datasets

(e.g., ETTh1 and ETTh2). However, we designed our cross-attention module as a general, extensible concept to handle information beyond just calendar marks.

5. Conclusion

We presented MOHETS, a novel transformer-based time series forecasting model that addresses the challenges of long-horizon multivariate prediction through tailored architectural innovations. By integrating a shared time-domain expert and routed frequency-domain experts, our MoHE architecture enforces structural decomposition of global trends and local periodicities – a combination that standard MLP-based experts fail to achieve. Thus, MOHETS establishes a multi-scale receptive field: global dependencies are resolved via attention, sequence-level continuity via the shared convolution, and local spectral details via Fourier experts. Additionally, the multimodal cross-attention mechanism integrates exogenous covariate embeddings, improving robustness to non-stationary dynamics. MOHETS achieved remarkable performance on multiple benchmarks, as validated through extensive ablation experiments. Therefore, this work introduces advancements that position MOHETS as a state-of-the-art solution for real-world time-series forecasting, providing a scalable and robust framework for diverse temporal applications.

Acknowledgments

This work was supported in part by the Paulo Pinheiro de Andrade Fellowship. The opinions, hypotheses, conclusions, or recommendations expressed in this material are the authors' responsibility and do not necessarily reflect the views of the funding agencies.

Impact Statement

This work advances long-term multivariate time-series forecasting, a capability that can improve decision-making in energy systems, climate modeling, supply chain management, and public health by increasing predictive accuracy and computational efficiency. Although these improvements support positive social outcomes, such as reducing energy waste and improving disaster readiness, forecasting models also carry risks. In particular, they can reproduce or amplify biases present in historical data, which may be misapplied in automated high-stakes decision systems without adequate human oversight. To mitigate these risks, we emphasize the need for rigorous validation, transparency in data provenance, and human oversight in deployment. We are not aware of any malicious applications specific to this research beyond those common to forecasting systems, but we encourage practitioners to apply domain-appropriate safeguards before operational deployment.

References

Ainslie, J., Lee-Thorp, J., De Jong, M., Zemlyanskiy, Y., Lebrón, F., and Sanghi, S. GQA: Training generalized multi-query transformer models from multi-head checkpoints. *arXiv preprint arXiv:2305.13245*, 2023.

Alexandrov, A., Benidis, K., Bohlke-Schneider, M., Flunkert, V., Gasthaus, J., Januschowski, T., Maddix, D. C., Rangapuram, S., Salinas, D., Schulz, J., Stella, L., Turkmen, A. C., and Wang, Y. GluonTS: Probabilistic and neural time series modeling in Python. *Journal of Machine Learning Research*, 21(116):1–6, 2020.

Ansari, A. F., Stella, L., Turkmen, C., Zhang, X., Mercado, P., Shen, H., Shchur, O., Rangapuram, S. S., Arango, S. P., Kapoor, S., et al. Chronos: Learning the language of time series. *Transactions on Machine Learning Research*, 2024.

Ba, J. L., Kiros, J. R., and Hinton, G. E. Layer normalization. *arXiv preprint arXiv:1607.06450*, 2016.

Bao, F., Nie, S., Xue, K., Cao, Y., Li, C., Su, H., and Zhu, J. All are worth words: A ViT backbone for diffusion models. In *Proceedings of the IEEE/CVF Conference on Computer Vision and Pattern Recognition*, pp. 22669–22679, 2023.

Chen, M., Radford, A., Child, R., Wu, J., Jun, H., Luan, D., and Sutskever, I. Generative pretraining from pixels. In *International Conference on Machine Learning (ICML)*, pp. 1691–1703. PMLR, 2020.

Chowdhery, A., Narang, S., Devlin, J., Bosma, M., Mishra, G., Roberts, A., Barham, P., Chung, H. W., Sutton, C., Gehrmann, S., et al. Palm: Scaling language modeling with pathways. *Journal of Machine Learning Research*, 24(240):1–113, 2023.

Dai, D., Deng, C., Zhao, C., Xu, R., Gao, H., Chen, D., Li, J., Zeng, W., Yu, X., Wu, Y., et al. DeepSeekMoE: Towards ultimate expert specialization in mixture-of-experts language models. *arXiv preprint arXiv:2401.06066*, 2024.

Dao, T. FlashAttention-2: Faster attention with better parallelism and work partitioning. In *The Twelfth International Conference on Learning Representations*, 2023.

Dao, T., Fu, D., Ermon, S., Rudra, A., and Ré, C. FlashAttention: Fast and memory-efficient exact attention with IO-awareness. *Advances in Neural Information Processing Systems*, 35:16344–16359, 2022.

Das, A., Kong, W., Leach, A., Sen, R., and Yu, R. Long-term forecasting with TiDE: Time-series dense encoder. *arXiv preprint arXiv:2304.08424*, 2023.

Das, A., Kong, W., Sen, R., and Zhou, Y. A decoder-only foundation model for time-series forecasting. In *International Conference on Machine Learning (ICML)*, 2024.

Dong, Y., Li, G., Tao, Y., Jiang, X., Zhang, K., Li, J., Deng, J., Su, J., Zhang, J., and Xu, J. FAN: Fourier analysis networks. *arXiv preprint arXiv:2410.02675*, 2024.

Dosovitskiy, A., Beyer, L., Kolesnikov, A., Weissenborn, D., Zhai, X., Unterthiner, T., Dehghani, M., Minderer, M., Heigold, G., Gelly, S., et al. An image is worth 16x16 words: Transformers for image recognition at scale. *arXiv preprint arXiv:2010.11929*, 2020.

Erturk, E., Kamran, F., Abbaspourazad, S., Jewell, S., Sharma, H., Li, Y., Williamson, S., Foti, N. J., and Futoma, J. Beyond sensor data: Foundation models of behavioral data from wearables improve health predictions. In *Proceedings of the 42nd International Conference on Machine Learning (ICML)*. PMLR, 2025.

Fedus, W., Zoph, B., and Shazeer, N. Switch transformers: Scaling to trillion parameter models with simple and efficient sparsity. *Journal of Machine Learning Research*, 23(120):1–39, 2022.

Garza, A., Challu, C., and Mergenthaler-Canseco, M. TimeGPT-1. *arXiv preprint arXiv:2310.03589*, 2023.

Glorot, X. and Bengio, Y. Understanding the difficulty of training deep feedforward neural networks. In *Proceedings of the Thirteenth International Conference on Artificial Intelligence and Statistics*, pp. 249–256. JMLR Workshop and Conference Proceedings, 2010.

Goerg, G. Forecastable component analysis. In *International Conference on Machine Learning (ICML)*, 2013.

Gong, Y., Chung, Y.-A., and Glass, J. AST: Audio spectrogram transformer. *arXiv preprint arXiv:2104.01778*, 2021.

Goswami, M., Szafer, K., Choudhry, A., Cai, Y., Li, S., and Dubrawski, A. MOMENT: A family of open time-series foundation models. In *International Conference on Machine Learning (ICML)*, 2024.

Grattafiori, A., Dubey, A., Jauhri, A., Pandey, A., Kadian, A., Al-Dahle, A., Letman, A., Mathur, A., Schelten, A., Vaughan, A., et al. The Llama 3 herd of models. *arXiv preprint arXiv:2407.21783*, 2024.

Han, L., Chen, X.-Y., Ye, H.-J., and Zhan, D.-C. SOFTS: Efficient multivariate time series forecasting with series-core fusion. *Advances in Neural Information Processing Systems*, 37:64145–64175, 2024.

Hendrycks, D. and Gimpel, K. Gaussian error linear units (GELUs). *arXiv preprint arXiv:1606.08415*, 2016.

Huang, G., Sun, Y., Liu, Z., Sedra, D., and Weinberger, K. Q. Deep networks with stochastic depth. In *European Conference on Computer Vision*, pp. 646–661. Springer, 2016.

Huber, P. J. Robust estimation of a location parameter. In *Breakthroughs in statistics: Methodology and distribution*, pp. 492–518. Springer, 1992.

Jiang, A. Q., Sablayrolles, A., Roux, A., Mensch, A., Savary, B., Bamford, C., Chaplot, D. S., Casas, D. d. l., Hanna, E. B., Bressand, F., et al. Mixtral of experts. *arXiv preprint arXiv:2401.04088*, 2024.

Kaplan, J., McCandlish, S., Henighan, T., Brown, T. B., Chess, B., Child, R., Gray, S., Radford, A., Wu, J., and Amodei, D. Scaling laws for neural language models. *arXiv preprint arXiv:2001.08361*, 2020.

Lago, J., Marcjasz, G., De Schutter, B., and Weron, R. Forecasting day-ahead electricity prices: A review of state-of-the-art algorithms, best practices and an open-access benchmark. *Applied Energy*, 293:116983, 2021.

Lepikhin, D., Lee, H., Xu, Y., Chen, D., Firat, O., Huang, Y., Krikun, M., Shazeer, N., and Chen, Z. GShard: Scaling giant models with conditional computation and automatic sharding. In *International Conference on Learning Representations*, 2021.

Lim, B., Arik, S. Ö., Loeff, N., and Pfister, T. Temporal fusion transformers for interpretable multi-horizon time series forecasting. *International Journal of Forecasting*, 2021.

Liu, M., Zeng, A., Chen, M., Xu, Z., Lai, Q., Ma, L., and Xu, Q. SCINet: Time series modeling and forecasting with sample convolution and interaction. *Advances in Neural Information Processing Systems*, 35:5816–5828, 2022a.

Liu, X., Liu, J., Woo, G., Aksu, T., Liang, Y., Zimmermann, R., Liu, C., Savarese, S., Xiong, C., and Sahoo, D. Moirai-MoE: Empowering time series foundation models with sparse mixture of experts. *arXiv preprint arXiv:2410.10469*, 2024a.

Liu, Y., Wu, H., Wang, J., and Long, M. Non-stationary transformers: Exploring the stationarity in time series forecasting. In *Advances in Neural Information Processing Systems*, 2022b.

Liu, Y., Hu, T., Zhang, H., Wu, H., Wang, S., Ma, L., and Long, M. iTraformer: Inverted transformers are effective for time series forecasting. *arXiv preprint arXiv:2310.06625*, 2023.

Liu, Y., Qin, G., Huang, X., Wang, J., and Long, M. Timer-XL: Long-context transformers for unified time series forecasting. In *International Conference on Learning Representations (ICLR)*, 2024b.

Liu, Y., Zhang, H., Li, C., Huang, X., Wang, J., and Long, M. Timer: Transformers for time series analysis at scale. In *International Conference on Machine Learning (ICML)*, 2024c.

Liu, Z., Mao, H., Wu, C.-Y., Feichtenhofer, C., Darrell, T., and Xie, S. A ConvNet for the 2020s. In *Proceedings of the IEEE/CVF Conference on Computer Vision and Pattern Recognition*, pp. 11976–11986, 2022c.

Loshchilov, I. and Hutter, F. SGDR: Stochastic gradient descent with warm restarts. *arXiv preprint arXiv:1608.03983*, 2016.

Loshchilov, I. and Hutter, F. Decoupled weight decay regularization. *arXiv preprint arXiv:1711.05101*, 2017.

Lutsker, G., Sapir, G., Shilo, S., Merino, J., Godneva, A., Greenfield, J. R., Samocha-Bonet, D., Dhir, R., Gude, F., Mannor, S., Meirom, E., Xing, E. P., Chechik, G., Rossman, H., and Segal, E. A foundation model for continuous glucose monitoring data. *Nature*, 2026.

Ni, R., Lin, Z., Wang, S., and Fanti, G. Mixture-of-linear-experts for long-term time series forecasting. In *International Conference on Artificial Intelligence and Statistics*, pp. 4672–4680. PMLR, 2024.

Nie, Y., Nguyen, N. H., Sinthong, P., and Kalagnanam, J. A time series is worth 64 words: Long-term forecasting with transformers. *arXiv preprint arXiv:2211.14730*, 2022.

Nie, Y., Kong, Y., Dong, X., Mulvey, J. M., Poor, H. V., Wen, Q., and Zohren, S. A survey of large language models for financial applications: Progress, prospects and challenges. *arXiv preprint arXiv:2406.11903*, 2024.

Ortigossa, E. S., Dias, F. F., Nascimento, D. C., and Nonato, L. G. Time series information visualization – a review of approaches and tools. *IEEE Access*, 13:161653–161684, 2025.

Paszke, A., Gross, S., Massa, F., Lerer, A., Bradbury, J., Chanan, G., Killeen, T., Lin, Z., Gimelshein, N., Antiga, L., et al. PyTorch: An imperative style, high-performance deep learning library. In *Advances in Neural Information Processing Systems*, 2019.

Pope, R., Douglas, S., Chowdhery, A., Devlin, J., Bradbury, J., Heek, J., Xiao, K., Agrawal, S., and Dean, J. Efficiently scaling transformer inference. *Proceedings of Machine Learning and Systems*, 5:606–624, 2023.

Riquelme, C., Puigcerver, J., Mustafa, B., Neumann, M., Jenatton, R., Susano Pinto, A., Keysers, D., and Houlsby, N. Scaling vision with sparse mixture of experts. *Advances in Neural Information Processing Systems*, 34: 8583–8595, 2021.

Salinas, D., Flunkert, V., Gasthaus, J., and Januschowski, T. DeepAR: Probabilistic forecasting with autoregressive recurrent networks. *International Journal of Forecasting*, 2020.

Sen, R., Yu, H.-F., and Dhillon, I. S. Think globally, act locally: A deep neural network approach to high-dimensional time series forecasting. *Advances in Neural Information Processing Systems*, 32, 2019.

Shazeer, N. Fast transformer decoding: One write-head is all you need. *arXiv preprint arXiv:1911.02150*, 2019.

Shazeer, N., Mirhoseini, A., Maziarz, K., Davis, A., Le, Q., Hinton, G., and Dean, J. Outrageously large neural networks: The sparsely-gated mixture-of-experts layer. In *International Conference on Learning Representations*, 2017.

Shi, X., Wang, S., Nie, Y., Li, D., Ye, Z., Wen, Q., and Jin, M. Time-MoE: Billion-scale time series foundation models with mixture of experts. *arXiv preprint arXiv:2409.16040*, 2024.

Srivastava, N., Hinton, G., Krizhevsky, A., Sutskever, I., and Salakhutdinov, R. Dropout: a simple way to prevent neural networks from overfitting. *The Journal of Machine Learning Research*, 15(1):1929–1958, 2014.

Su, J., Ahmed, M., Lu, Y., Pan, S., Bo, W., and Liu, Y. RoFormer: Enhanced transformer with rotary position embedding. *Neurocomputing*, 568:127063, 2024.

Vaswani, A., Shazeer, N., Parmar, N., Uszkoreit, J., Jones, L., Gomez, A. N., Kaiser, Ł., and Polosukhin, I. Attention is all you need. In *Advances in Neural Information Processing Systems*, 2017.

Wang, S., Wu, H., Shi, X., Hu, T., Luo, H., Ma, L., Zhang, J. Y., and Zhou, J. TimeMixer: Decomposable multi-scale mixing for time series forecasting. In *The Twelfth International Conference on Learning Representations*, 2024a.

Wang, Y., Wu, H., Dong, J., Qin, G., Zhang, H., Liu, Y., Qiu, Y., Wang, J., and Long, M. TimeXer: Empowering transformers for time series forecasting with exogenous variables. *Advances in Neural Information Processing Systems*, 37:469–498, 2024b.

Wen, Q., Gao, J., Song, X., Sun, L., and Tan, J. RobustTrend: a huber loss with a combined first and second order difference regularization for time series trend filtering. In *Proceedings of the 28th International Joint Conference on Artificial Intelligence*, pp. 3856–3862, 2019.

Wen, Q., Zhou, T., Zhang, C., Chen, W., Ma, Z., Yan, J., and Sun, L. Transformers in time series: a survey. In *Proceedings of the Thirty-Second International Joint Conference on Artificial Intelligence (IJCAI)*, pp. 6778–6786, 2023.

Woo, G., Liu, C., Kumar, A., Xiong, C., Savarese, S., and Sahoo, D. Unified training of universal time series forecasting transformers. In *Forty-first International Conference on Machine Learning (ICML)*, 2024.

Wu, H., Xiao, B., Codella, N., Liu, M., Dai, X., Yuan, L., and Zhang, L. CvT: Introducing convolutions to vision transformers. *arXiv preprint arXiv:2103.15808*, 2021a.

Wu, H., Xu, J., Wang, J., and Long, M. Autoformer: Decomposition transformers with auto-correlation for long-term series forecasting. In *Advances in Neural Information Processing Systems*, 2021b.

Wu, H., Hu, T., Liu, Y., Zhou, H., Wang, J., and Long, M. TimesNet: Temporal 2d-variation modeling for general time series analysis. In *International Conference on Learning Representations (ICLR)*, 2023.

Wu, Y. and He, K. Group normalization. In *Proceedings of the European Conference on Computer Vision (ECCV)*, pp. 3–19, 2018.

Xiong, R., Yang, Y., He, D., Zheng, K., Zheng, S., Xing, C., Zhang, H., Lan, Y., Wang, L., and Liu, T. On layer normalization in the transformer architecture. In *International Conference on Machine Learning (ICML)*, pp. 10524–10533. PMLR, 2020.

Zeng, A., Chen, M., Zhang, L., and Xu, Q. Are transformers effective for time series forecasting? In *Proceedings of the AAAI Conference on Artificial Intelligence*, 2023.

Zhang, B. and Sennrich, R. Root mean square layer normalization. *Advances in Neural Information Processing Systems*, 32, 2019.

Zhang, Y. and Yan, J. Crossformer: Transformer utilizing cross-dimension dependency for multivariate time series forecasting. In *International Conference on Learning Representations (ICLR)*, 2022.

Zhang, Y., Long, M., Chen, K., Xing, L., Jin, R., Jordan, M. I., and Wang, J. Skilful nowcasting of extreme precipitation with NowcastNet. *Nature*, 2023.

Zhou, H., Zhang, S., Peng, J., Zhang, S., Li, J., Xiong, H., and Zhang, W. Informer: Beyond efficient transformer for long sequence time-series forecasting. In *Proceedings of the AAAI Conference on Artificial Intelligence*, 2021.

Zhou, T., Ma, Z., Wen, Q., Wang, X., Sun, L., and Jin, R. FEDformer: Frequency enhanced decomposed transformer for long-term series forecasting. In *International Conference on Machine Learning (ICML)*, 2022.

A. Experimental Details

A.1. Dataset Descriptions

We conduct long-term multivariate forecasting experiments on 7 well-established real-world datasets to evaluate the performance of our MOHETS, including: the ETT (Zhou et al., 2021) series that contains four subsets with seven features related to power load of electricity transformers recorded during two years, where ETTh1 and ETTh2 are recorded hourly, and ETTm1 and ETTm2 are recorded every 15 minutes; Weather (Wu et al., 2021b) that includes 21 meteorological features collected every 10 minutes from the Max Planck Institute for Biogeochemistry; ECL (Wu et al., 2021b) that contains hourly electricity consumption records from 321 clients; and Traffic (Wu et al., 2021b) records hourly road occupancy rates from 862 sensors on San Francisco Bay freeways. These datasets are publicly available and have been extensively utilized for benchmarking time series forecasting models. The statistics of each dataset are provided in Table 5.

Table 5. Dataset descriptions. Dim denotes the number of variables. Dataset size refers to the number of time points and is organized into (Train, Validation, Test) splits.

Task	Dataset	Dim	Dataset Size	Frequency	Forecastability	Information
Long-term Forecasting	ETTh1	7	(8545, 2881, 2881)	1 Hour	0.38	Power Load
	ETTh2	7	(8545, 2881, 2881)	1 Hour	0.45	Power Load
	ETTm1	7	(34465, 11521, 11521)	15 Min	0.46	Power Load
	ETTm2	7	(34465, 11521, 11521)	15 Min	0.55	Power Load
	Weather	21	(36792, 5271, 10540)	10 Min	0.75	Weather
	ECL	321	(18317, 2633, 5261)	1 Hour	0.77	Electricity
	Traffic	862	(12185, 1757, 3509)	1 Hour	0.68	Transportation

Forecastability (Goerg, 2013) is a measure of future uncertainty computed by one minus the entropy of the Fourier decomposition of time series. Higher values indicate better levels of predictability.

A.2. Baseline Models

We select 15 advanced, well-known models as baselines for each experiment, representing the state-of-the-art in time series forecasting. These baselines include Transformer-based models such as TimeXer (Wang et al., 2024b), iTransformer (Liu et al., 2023), PatchTST (Nie et al., 2022), Crossformer (Zhang & Yan, 2022), FEDformer (Zhou et al., 2022), Timer-XL (Liu et al., 2024b), Time-MoE (Shi et al., 2024), Moirai (Woo et al., 2024), MOMENT (Goswami et al., 2024), and Chronos (Ansari et al., 2024), as well as SOFTS (Han et al., 2024), TimeMixer (Wang et al., 2024a), TiDE (Das et al., 2023), and DLinear (Zeng et al., 2023), which are based on MLP layers, and TimesNet (Wu et al., 2023), which is based on 2D convolutions. In particular, Timer-XL, TiDE, and TimeXer are recently published forecasters specifically designed to encode historical time series along with exogenous information.

SOFTS, TimeXer, iTransformer, TimeMixer, TimesNet, PatchTST, Crossformer, FEDformer, TiDE, and DLinear are in-domain (full-shot) time series models. On the other hand, Timer-XL, Time-MoE, Moirai, MOMENT, and Chronos are large time-series foundation models pre-trained on multiple time-series datasets. In particular, Time-MoE is a mixture-of-experts Transformer with three model versions that scale to more than two billion parameters, pre-trained on a vast database comprising over 300 billion time points (Shi et al., 2024). We report the official results from (Liu et al., 2023; Wang et al., 2024b; Han et al., 2024; Liu et al., 2024c).

A.3. Metrics

We use the mean squared error (MSE) and mean absolute error (MAE) as evaluation metrics for the time-series forecasting experiments. A lower MSE or MAE indicates a better prediction. These metrics are calculated as follows:

$$\text{MSE} = \frac{1}{H} \sum_{t=1}^H (\mathbf{x}_t - \hat{\mathbf{x}}_t)^2, \quad \text{MAE} = \frac{1}{H} \sum_{t=1}^H |\mathbf{x}_t - \hat{\mathbf{x}}_t|,$$

where $\mathbf{x}_t, \hat{\mathbf{x}}_t \in \mathbb{R}$ are the ground truth and the corresponding prediction of the t -th future time point. We further calculate the mean metric in the variable dimension for multivariate time series.

A.4. Hyperparameter Settings

With the settings defined in Sectio 3.9, we propose four model variants: MOHETS_{tiny}, with 0.3 million activated parameters; MOHETS_{small}, with 1.3 million activated parameters; MOHETS_{base}, with 7.4 million activated parameters; and MOHETS_{large}, with 21.4 million activated parameters; all versions are designed for efficient inference on CPU architectures and significantly lighter compared to current state-of-the-art models in long-term time series forecasting (Shi et al., 2024; Liu et al., 2024a; Das et al., 2024). The detailed model configurations are in Table 6.

Table 6. Summary of MoHETS model configurations. Total Params can vary according to the data dimensionality.

	Blocks	Q-Heads	KV-Heads	Experts	K	d_{model}	d_{ff}	Activated Params	Total Params
MOHETS _{tiny}	4	4	2	8	2	64	128	0.3 M	0.6 M
MOHETS _{small}	4	4	2	8	2	128	256	1.3 M	2.5 M
MOHETS _{base}	6	8	4	8	2	256	512	7.4 M	14.5 M
MOHETS _{large}	8	12	6	8	2	384	768	21.4 M	42.7 M

For all experiments, we define a standard base frequency of 10,000 for Rotary Position Embeddings (RoPE). We apply DropPath (Huang et al., 2016) with stochastic decay to the output of the attention and MoHE modules according to the depth of their Transformer blocks, with a maximum probability of 0.3. We also apply Dropout (Srivastava et al., 2014) with probability 0.2 to other encoder components. Furthermore, we use xavier_uniform (Glorot & Bengio, 2010) to initialize all the learnable weights of our model, except the Fourier Feed Forward networks in MoHE modules, which we initialize using normal distributions. The reason for this choice lies in the trigonometric nature of the Fourier layers (Dong et al., 2024), which use explicit periodic cos and sin components to model periodic frequencies.

Widely used initializations such as xavier_ and kaiming_ are not ideal for periodic projections because they are designed to preserve variance for ReLU-style flows, but not for cos and sin operations. In practice, these initializations tend to produce distributions that are either too small or too structured, leading to periodic paths collapsing to near-constant behaviors. Therefore, initialization must place the weights of the Fourier layers in a moderate range, with $\mathcal{N}(0, 1)$ ensuring that during the first forward pass, the periodic features are well distributed to enable different phases (i.e., non-trivial), preventing them from collapsing near zero. **The code will be publicly available on GitHub upon acceptance.**

A.5. Technical Details

Attention. In MoHETS, we implement grouped-query attention (GQA) (Ainslie et al., 2023) to optimize self-attention and cross-attention mechanisms, balancing computational efficiency and modeling capacity. Standard multi-head attention (MHA) (Vaswani et al., 2017) allocates independent query (Q), key (K), and value (V) projections to each attention head, generating rich contextual information. The downside of MHA is the high memory bandwidth and computational costs, particularly for long sequences and autoregressive inference. Multi-query attention (MQA) (Shazeer, 2019) was proposed to mitigate attention costs by using a single K and V projection on multiple query heads, drastically reducing the memory footprint. However, this abrupt reduction in the K and V projections can degrade the model’s capacity and training stability due to restricted representational expressivity, leading to a reduced performance compared to MHA (Ainslie et al., 2023).

GQA addresses the efficiency and capacity trade-off with a more general and flexible formulation of MHA that groups query heads into tunable clusters, each cluster sharing a single K and V projection, thereby reducing memory while preserving performance close to MHA (Ainslie et al., 2023). GQA has been successfully adopted in large-scale models, demonstrating improved efficiency with minimal loss of quality (Grattafiori et al., 2024). For time series forecasting, long horizons require efficient attention. Thus, we adopt a light query grouping factor of 2 in MoHETS, that is, Q-heads = 2 × KV-heads (see Figure 2 and Table 6), which, combined with FlashAttention (Dao et al., 2022), reduces memory overhead while maintaining robust modeling capacity.

MoHE Components. Our Mixture-of-Heterogeneous-Experts approach consists of one shared expert designed to capture sequence-level temporal patterns and multiple routed experts designed to model patch-level periodic patterns. All experts are randomly initialized. During training, the router learns to send similar patches to the same experts. Only selected experts

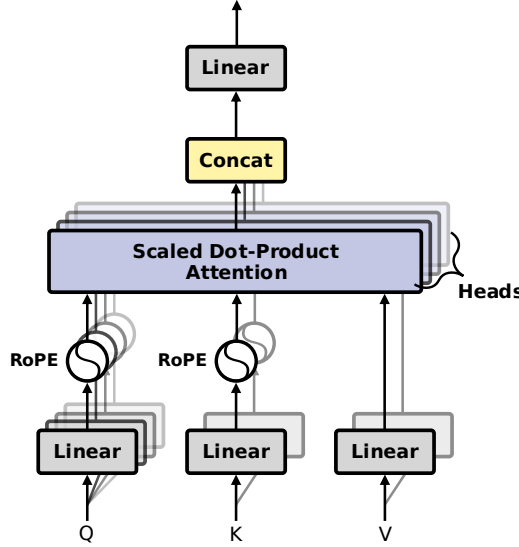


Figure 2. The grouped-query attention (GQA) mechanism with Rotary Position Embeddings (RoPE). Single key and value heads are shared for each group of query heads. In MoHETS, we adopt a grouping factor of two query heads for each key/value head, i.e., Q-heads = 2 × KV-heads.

will receive gradient updates and specialize in processing that type of patch. The routing mechanism operates independently in each MoHE layer along the model, creating a sophisticated network of specialization. For an input patch embedding p , the shared expert’s contribution is gated by the weight $g_{N+1,p}$, computed using the Sigmoid function (Equation 10). In contrast, the routed experts use the Topk Softmax routing weights $g_{i,p}$, as defined in Equations 5 and 6, retaining only the K highest scores to ensure sparsity. The final output combines the contributions of both shared and Topk experts to capture long-term patterns and local periodicity (see Figure 1c). The MoHE architecture activates only relevant parts of the model for each time patch, enabling model scaling without a corresponding increase in computation. It should be noted that we did not experiment with all convolutional experts because it does not make sense to process data units (single patches) using convolutions.

Fourier-based Networks. Multi-layer perceptron (MLP) networks are widely used in machine learning and deep learning models, due to their general-purpose ability to approximate diverse functions. However, this general nature can hinder MLPs in accurately modeling patterns such as periodic signals (Dong et al., 2024). In our MoHE modules, we replace the standard MLP-FFNs in routed experts with Fourier analysis networks (FA-FFNs). An FA-FFN is composed of two layers, following the typical inverted bottleneck design of Transformer blocks. Each layer is based on the Fourier series, which decomposes inputs into frequency-domain representations using sines and cosines, enhancing periodicity modeling. The FA-FFN is defined as follows:

$$\text{FA-FFN}(\mathbf{x}) = \phi_{L2} \circ \phi_{L1} \circ \mathbf{x}, \quad (12)$$

with

$$\phi_l(\mathbf{x}) = [\cos(W_p^l \mathbf{x}) || \sin(W_p^l \mathbf{x}) || \sigma(W_{\bar{p}}^l \mathbf{x} + b_{\bar{p}}^l)], \quad (13)$$

where $W_p \in \mathbb{R}^{d_{\text{model}} \times d_{\text{ff}}/4}$, $W_{\bar{p}} \in \mathbb{R}^{d_{\text{model}} \times d_{\text{ff}}/2}$, and $b_{\bar{p}} \in \mathbb{R}^{d_{\text{ff}}/2}$ are learnable parameters, σ is a GELU activation function, and $||$ denotes concatenation. Note that an MLP layer is a special case of Equation 13 when the W_p parameters are learned to be zero, which means that an FA-FFN is designed to model periodic signals, but can also retain general-purpose modeling capabilities as standard FFN (Dong et al., 2024).

Prediction Loss. Time series forecasting models are often trained using the MSE loss. We deviate and use the Huber loss (Huber, 1992; Wen et al., 2019), which combines the advantages of the L1 and MSE losses to provide robustness to outliers, improving training stability (Shi et al., 2024). For predicted time points $\hat{\mathbf{x}}_t$ and ground truth \mathbf{x}_t , the Huber loss is defined as:

$$\mathcal{L}_{\text{pred}}(\mathbf{x}_t, \hat{\mathbf{x}}_t) = \begin{cases} 0.5 (\mathbf{x}_t - \hat{\mathbf{x}}_t)^2, & \text{if } |\mathbf{x}_t - \hat{\mathbf{x}}_t| \leq \delta, \\ \delta \times (|\mathbf{x}_t - \hat{\mathbf{x}}_t| - 0.5 \times \delta), & \text{otherwise,} \end{cases} \quad (14)$$

with δ as a hyperparameter that balances the scaled L1 and MSE losses. As demonstrated by (Shi et al., 2024), time series models trained with Huber loss outperform those trained using only MSE loss due to the superior robustness of Huber loss in handling outliers.

Expert Balance Loss. Sparse Mixture-of-Experts architectures, such as our MoHE, rely on automatically learned routing strategies that may suffer from load imbalance where a few experts dominate patch assignments. As a consequence, the routing can collapse, leading to under-utilization of experts and reduced specialization (Shi et al., 2024; Dai et al., 2024). To avoid the risk of routing collapse, we incorporate the auxiliary expert balance loss proposed by (Fedus et al., 2022). This loss penalizes experts with high gating scores, promoting balanced loads among experts to prevent stronger experts from monopolizing patches during training, being computed as:

$$\mathcal{L}_{\text{aux}} = N \sum_{i=1}^N f_i r_i, \quad (15)$$

where f_i denotes the fraction of input patches routed to expert i , and r_i represents the average routing score allocated to expert i by the gating mechanism. These quantities are formally defined as:

$$f_i = \frac{1}{KP} \sum_{p=1}^P \mathbb{I}(\text{Time patch } p \text{ selects Expert } i), \quad r_i = \frac{1}{P} \sum_{p=1}^P s_{i,p}, \quad (16)$$

where P is the number of input patches, K is the number of experts selected per time patch, $s_{i,p}$ is the expert routing probability (from Softmax score, see Equation 6), and \mathbb{I} is the indicator function (Dai et al., 2024). Therefore, the expert balance loss is calculated as the product of the fraction of patches, f_i , routed to each expert i , and the routing probability, r_i , thereby encouraging uniform expert utilization by assigning higher loss values to experts with higher routing probabilities.

Output Head Architecture. As illustrated in Figure 1d, we apply a final RMSNorm to the last Transformer block to improve stability and then forward the resulting patch embedding to the output decoder module, which is designed as follows. A single-layer MLP with dimensions $d_{\text{model}} \times d_{\text{model}}$ receives the normalized embeddings, and a ConvTranspose layer unpatches each embedding to time points. The unpatched sequence is processed and projected by a convolutional block inspired by ConvNeXt’s large kernel inverted bottleneck (Liu et al., 2022c), i.e., (i) a depthwise convolution with default kernel size of 7 to focus on non-local temporal interactions at the sequence level, followed by a single-group GroupNorm along the channel dimension to normalize embeddings; (ii) a pointwise convolution reducing the dimension by a factor of 4 followed by a GELU activation; and (iii) a final pointwise convolution projecting the embedding to a single dimension. Finally, channel-independent outputs are reshaped to the original data dimension, $\mathbb{R}^{D \times H}$.

In Figure 3, we compare training and validation loss curves of MoHETS on the Traffic dataset ($\text{MOHETS}_{\text{small}}$, $P = 12$, $H_o = 24$, and 20 epochs of training), using a conventional MLP projection head (left) and our proposed convolutional decoder head (right). The convolutional head version achieves smoother training optimization compared to the oscillatory validation loss decrease observed in the MLP head version, leading MoHETS to an average forecasting MSE of 0.406, compared to 0.418 for the MLP head (see Table 4). Furthermore, the convolutional design is more parameter-efficient, reducing the total number of parameters by 42% (from 4.7M parameters to 8.1M parameters for the MLP head version), indicating that the convolutional decoder improves generalization and reduces the model size.

B. Full Experimental Results

In Table 7, we provide the full results for each forecasting task in Table 1. We highlight the performance of MoHETS in ultra-long-horizon multivariate forecasting tasks, that is, predicting 720 future time points, where our model outperforms TimeXer by an 11.7% reduction in MSE on the ETTh1 dataset and by an 11.2% reduction in MSE on ETTh2, in addition to also outperforming TimeMixer by a 10.6% reduction in MSE on the Weather data and TimeXer by a 3.8% reduction in MSE on ECL. These consistent gains underscore MoHETS’s robustness for extended forecasting.

In Table 8, we present additional comparisons with time series foundation models to provide a more comprehensive evaluation. Specifically, we include Timer-XL, and all versions of Time-MoE, Moirai, MOMENT, and Chronos (see Section A.2). It should be noted that Time-MoE and Moirai achieve strong results on the ETTh1 and ETTh2 datasets. These datasets are small and coarse-grained, making them prone to overfitting even with models of moderate size (Nie et al., 2022), suggesting that pre-training on large-scale time series is a valuable approach to enhance performance in such contexts.

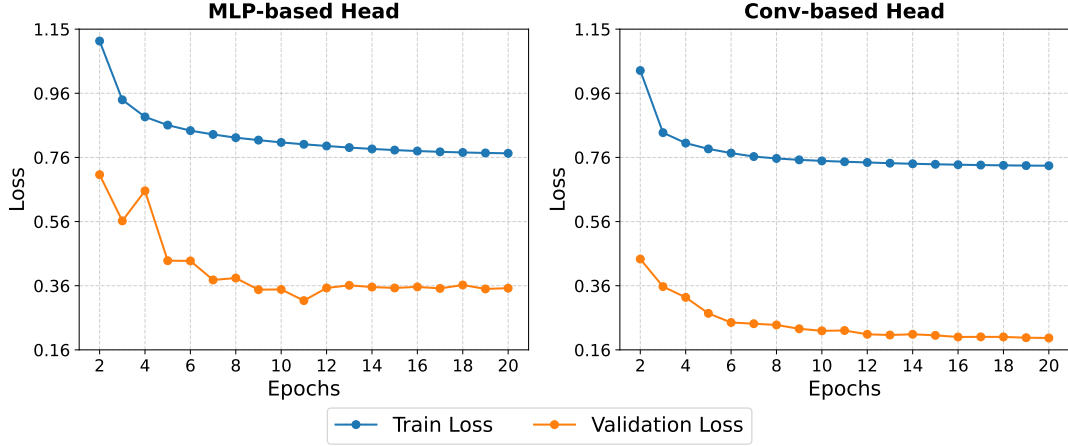


Figure 3. Training and validation loss curves of MoHETS on Traffic data, comparing a conventional MLP-based projection head (left) with our convolutional head (right). We combine the Huber loss with the balanced loss for training (see Section 3.8) and use the MSE loss for validation.

Table 7. Results of long-term multivariate forecasting experiments. Full-shot results are obtained from (Liu et al., 2023; Wang et al., 2024b; Han et al., 2024). **Bold red**: the best, underlined blue: the second best. 1st Count represents the number of wins achieved by a model across all prediction lengths and datasets.

Models	MOHETS		SOFTS		TimeXer		iTransformer		TimeMixer		TimesNet		PatchTST		Crossformer		TiDE		DLinear		FEDformer	
Metrics ↓	MSE	MAE	MSE	MAE	MSE	MAE	MSE	MAE	MSE	MAE	MSE	MAE	MSE	MAE	MSE	MAE	MSE	MAE	MSE	MAE	MSE	MAE
ETTh1	96	0.350 0.383	0.381 <u>0.399</u>	0.382 0.403	0.386 0.405	<u>0.375</u> 0.400	0.384 0.402	0.414 0.419	0.423 0.448	0.479 0.464	0.386 0.400	0.376 0.419										
	192	0.376 0.404	0.435 0.431	0.429 0.435	0.441 0.436	0.436 <u>0.429</u>	0.421 <u>0.429</u>	0.460 0.445	0.471 0.474	0.525 0.492	0.437 0.432	0.420 0.448										
	336	0.393 0.418	0.480 0.452	0.468 <u>0.448</u>	0.487 0.458	0.484 0.458	0.491 0.469	0.501 0.466	0.570 0.546	0.565 0.515	0.481 0.459	0.459 0.465										
	720	0.414 0.441	0.499 0.488	<u>0.469</u> <u>0.461</u>	0.503 0.491	0.498 0.482	0.521 0.500	0.500 0.488	0.653 0.621	0.594 0.558	0.519 0.516	0.506 0.507										
	Avg.	0.383 0.412	0.449 0.442	<u>0.437</u> <u>0.437</u>	0.454 0.447	0.448 0.442	0.454 0.450	0.469 0.454	0.529 0.522	0.540 0.507	0.455 0.451	0.440 0.459										
ETTh2	96	0.278 0.332	0.297 0.347	<u>0.286</u> <u>0.338</u>	0.297 0.349	0.289 0.341	0.340 0.374	0.302 0.348	0.745 0.584	0.400 0.440	0.333 0.387	0.358 0.397										
	192	0.345 0.374	0.373 0.394	<u>0.363</u> <u>0.389</u>	0.380 0.400	0.372 0.392	0.402 0.414	0.388 0.400	0.877 0.656	0.528 0.509	0.477 0.476	0.429 0.439										
	336	0.376 0.400	0.410 0.426	0.414 0.423	0.428 0.432	<u>0.386</u> <u>0.414</u>	0.452 0.541	0.426 0.433	1.043 0.731	0.643 0.571	0.594 0.541	0.496 0.487										
	720	0.392 0.421	0.411 0.433	<u>0.408</u> <u>0.432</u>	0.427 0.445	0.412 0.434	0.462 0.657	0.431 0.446	1.104 0.763	0.874 0.679	0.831 0.657	0.463 0.474										
	Avg.	0.348 0.382	0.373 0.400	0.367 0.396	0.383 0.406	<u>0.364</u> <u>0.395</u>	0.414 0.496	0.387 0.407	0.942 0.683	0.611 0.549	0.558 0.515	0.436 0.449										
ETTm1	96	0.276 0.327	0.325 0.361	<u>0.318</u> <u>0.356</u>	0.334 0.368	0.320 0.357	0.338 0.375	0.329 0.367	0.404 0.426	0.364 0.387	0.345 0.372	0.379 0.419										
	192	0.313 0.354	0.375 0.389	0.362 0.383	0.377 0.391	<u>0.361</u> <u>0.381</u>	0.374 0.387	0.367 0.385	0.450 0.451	0.398 0.404	0.380 0.389	0.426 0.441										
	336	0.343 0.376	0.405 0.412	0.395 0.407	0.426 0.420	<u>0.390</u> <u>0.404</u>	0.410 0.411	0.399 0.410	0.532 0.515	0.428 0.425	0.413 0.413	0.445 0.459										
	720	0.401 0.410	0.466 0.447	<u>0.452</u> 0.441	0.491 0.459	0.454 0.441	0.478 0.450	0.454 0.439	0.666 0.589	0.487 0.461	0.474 0.453	0.543 0.490										
	Avg.	0.333 0.367	0.393 0.403	0.382 0.397	0.407 0.410	<u>0.381</u> <u>0.395</u>	0.400 0.405	0.387 0.400	0.513 0.495	0.419 0.419	0.403 0.406	0.448 0.452										
ETTm2	96	0.164 0.249	0.180 0.261	<u>0.171</u> <u>0.256</u>	0.180 0.264	0.175 0.258	0.187 0.267	0.175 0.259	0.287 0.366	0.207 0.305	0.193 0.292	0.203 0.287										
	192	0.222 0.288	0.246 0.306	<u>0.237</u> <u>0.299</u>	0.250 0.309	<u>0.237</u> <u>0.299</u>	0.249 0.309	0.241 0.302	0.414 0.492	0.290 0.364	0.284 0.362	0.269 0.328										
	336	0.275 0.323	0.319 0.352	<u>0.296</u> <u>0.338</u>	0.311 0.348	0.298 0.340	0.321 0.351	0.305 0.343	0.597 0.542	0.377 0.422	0.369 0.427	0.325 0.366										
	720	0.361 0.378	0.405 0.401	0.392 <u>0.394</u>	0.412 0.407	<u>0.391</u> 0.396	0.408 0.403	0.402 0.400	1.730 1.042	0.558 0.524	0.554 0.522	0.421 0.415										
	Avg.	0.256 0.310	0.287 0.330	<u>0.274</u> <u>0.322</u>	0.288 0.332	0.275 0.323	0.291 0.332	0.281 0.326	0.757 0.610	0.358 0.403	0.350 0.400	0.304 0.349										
Weather	96	0.141 0.184	0.166 0.208	<u>0.157</u> <u>0.205</u>	0.174 0.214	0.163 0.209	0.172 0.220	0.177 0.218	0.158 0.230	0.202 0.261	0.196 0.255	0.217 0.296										
	192	0.184 0.227	0.217 0.253	<u>0.204</u> <u>0.247</u>	0.221 0.254	0.208 0.250	0.219 0.261	0.225 0.259	0.206 0.277	0.242 0.298	0.237 0.296	0.276 0.336										
	336	0.235 0.268	0.282 0.300	0.261 0.290	0.278 0.296	<u>0.251</u> <u>0.287</u>	0.280 0.306	0.278 0.297	0.272 0.335	0.287 0.335	0.283 0.335	0.339 0.380										
	720	0.303 0.318	0.356 0.351	0.340 <u>0.341</u>	0.358 0.349	<u>0.339</u> <u>0.341</u>	0.365 0.359	0.354 0.348	0.398 0.418	0.351 0.386	0.345 0.381	0.403 0.428										
	Avg.	0.216 0.249	0.255 0.278	0.241 <u>0.271</u>	0.258 0.278	<u>0.240</u> <u>0.271</u>	0.259 0.286	0.259 0.281	0.258 0.315	0.270 0.320	0.265 0.316	0.308 0.360										
ECL	96	0.125 0.218	0.143 <u>0.233</u>	<u>0.140</u> 0.242	0.148 0.240	0.153 0.247	0.168 0.272	0.181 0.270	0.219 0.314	0.237 0.329	0.197 0.282	0.193 0.308										
	192	0.144 0.236	0.158 <u>0.248</u>	<u>0.157</u> 0.256	0.162 0.253	0.166 0.256	0.184 0.289	0.188 0.274	0.231 0.322	0.236 0.330	0.196 0.285	0.201 0.315										
	336	0.161 0.256	0.178 <u>0.269</u>	<u>0.176</u> 0.275	0.178 <u>0.269</u>	0.185 0.277	0.198 0.300	0.204 0.293	0.246 0.337	0.249 0.344	0.209 0.301	0.214 0.329										
	720	0.203 0.295	0.218 <u>0.305</u>	<u>0.211</u> 0.306	0.225 0.317	0.225 0.310	0.220 0.320	0.246 0.324	0.280 0.363	0.284 0.373	0.245 0.333	0.246 0.355										
	Avg.	0.158 0.251	0.174 <u>0.264</u>	<u>0.171</u> 0.270	0.178 0.270	0.182 0.272	0.192 0.295	0.205 0.290	0.244 0.334	0.251 0.344	0.212 0.300	0.214 0.327										
Traffic	96	0.351 0.236	<u>0.376</u> <u>0.251</u>	0.428 0.271	0.395 0.268	0.462 0.285	0.593 0.321	0.462 0.295	0.522 0.290	0.805 0.493	0.650 0.396	0.587 0.366										
	192	0.372 0.247	<u>0.398</u> <u>0.261</u>	0.448 0.282	0.417 0.276	0.473 0.296	0.617 0.336	0.466 0.296	0.530 0.293	0.756 0.474	0.598 0.370	0.604 0.373										
	336	0.391 0.257	<u>0.415</u> <u>0.269</u>	0.473 0.289	0.433 0.283	0.498 0.296	0.629 0.336	0.482 0.304	0.558 0.305	0.762 0.477	0.605 0.373	0.621 0.383										
	720	0.440 0.284	<u>0.447</u> <u>0.287</u>	0.516 0.307	0.467 0.302	0.506 0.313	0.640 0.350	0.514 0.322	0.589 0.328	0.719 0.449	0.645 0.394	0.626 0.382										
	Avg.	0.388 0.256	<u>0.409</u> <u>0.267</u>	0.466 0.287	0.428 0.282	0.484 0.297	0.620 0.336	0.481 0.304	0.550 0.304	0.760 0.473	0.625 0.383	0.609 0.376										
Average		0.297 0.318	<u>0.334</u> 0.341	<u>0.334</u> <u>0.340</u>	0.342 0.346	0.339 0.342	0.376 0.371	0.353 0.352	0.542 0.466	0.458 0.431	0.410 0.396	0.394 0.396										
1st Count		72	0	0	0	0	0	0	0	0	0	0										

In particular, Time-MoE, a foundation model pre-trained on a vast time-series dataset, outperforms MoHETS across a

few horizons. However, MoHETS outperforms Time-MoE in most benchmarks, including a 15.6% reduction in average MSE on the Weather data relative to Time-MoE_{ultra}. We highlight that MoHETS is considerably lighter, demonstrating that combining carefully designed architectures to capture heterogeneous patterns from time series enables MoHETS to achieve state-of-the-art performance efficiently. The general results in Table 8 indicate that our model performs consistently against such established approaches, including the 2.4-billion-parameter Time-MoE_{ultra}.

Table 8. Additional results of long-term multivariate forecasting against large foundation model baselines. Results are obtained from (Liu et al., 2024c). **Bold red**: the best, underlined blue: the second best. 1st Count represents the number of wins achieved by a model across all prediction lengths and datasets.

Models	MoHETS	Timer-XL _{Base}	Time-MoE _{Base}	Time-MoE _{Large}	Time-MoE _{Ultra}	Moirai _{Small}	Moirai _{Base}	Moirai _{Large}	MOMENT	Chronos _{Base}	Chronos _{Large}	
Metrics ↓	MSE MAE	MSE MAE	MSE MAE	MSE MAE	MSE MAE	MSE MAE	MSE MAE	MSE MAE	MSE MAE	MSE MAE	MSE MAE	
ETTh1	96 0.350 0.383	0.369 0.391	0.357 0.381	0.350 0.382	0.349 0.379	0.401 0.402	0.376 0.392	0.381 0.388	0.688 0.557	0.440 0.393	0.441 0.390	
	192 0.376 0.404	0.405 0.413	0.384 0.404	0.388 0.412	0.395 0.413	0.435 0.421	0.412 0.413	0.434 0.415	0.688 0.560	0.492 0.426	0.502 0.524	
	336 0.393 0.418	0.418 0.423	0.411 0.434	0.411 0.430	0.447 0.453	0.438 0.434	0.433 0.428	0.485 0.445	0.675 0.563	0.550 0.462	0.576 0.467	
	720 0.414 0.441	0.423 0.441	0.449 0.477	0.427 0.455	0.457 0.462	0.439 0.454	0.447 0.444	0.611 0.510	0.683 0.585	0.882 0.591	0.835 0.583	
Avg.		0.383 0.412	0.404 0.417	0.400 0.424	0.394 0.419	0.412 0.426	0.428 0.427	0.417 0.419	0.480 0.439	0.683 0.566	0.591 0.468	0.588 0.466
ETTh2	96 0.278 0.332	0.283 0.342	0.305 0.359	0.302 0.354	0.292 0.352	0.297 0.336	0.294 0.330	0.296 0.330	0.342 0.396	0.308 0.343	0.320 0.345	
	192 0.345 0.374	0.340 0.379	0.351 0.386	0.364 0.385	0.347 0.379	0.368 0.381	0.363 0.375	0.361 0.371	0.354 0.402	0.384 0.392	0.406 0.399	
	336 0.376 0.400	0.366 0.400	0.391 0.418	0.417 0.425	0.406 0.419	0.370 0.393	0.376 0.390	0.390 0.390	0.407 0.407	0.429 0.430	0.492 0.453	
	720 0.392 0.421	0.397 0.431	0.419 0.454	0.537 0.496	0.439 0.447	0.411 0.426	0.416 0.433	0.423 0.418	0.434 0.434	0.501 0.477	0.603 0.511	
Avg.		0.348 0.382	0.347 0.388	0.366 0.404	0.405 0.415	0.371 0.399	0.361 0.384	0.362 0.382	0.367 0.377	0.361 0.409	0.405 0.410	0.455 0.427
ETTm1	96 0.276 0.327	0.317 0.356	0.338 0.368	0.309 0.357	0.281 0.341	0.418 0.392	0.363 0.356	0.380 0.361	0.654 0.527	0.454 0.408	0.457 0.403	
	192 0.313 0.354	0.358 0.381	0.353 0.388	0.346 0.381	0.305 0.358	0.431 0.405	0.388 0.375	0.412 0.383	0.662 0.532	0.567 0.477	0.530 0.450	
	336 0.343 0.376	0.386 0.401	0.381 0.413	0.373 0.408	0.369 0.395	0.433 0.412	0.416 0.392	0.436 0.400	0.672 0.537	0.662 0.525	0.577 0.481	
	720 0.401 0.410	0.430 0.431	0.504 0.493	0.475 0.477	0.469 0.472	0.462 0.432	0.460 0.418	0.462 0.420	0.692 0.551	0.900 0.591	0.660 0.526	
Avg.		0.333 0.367	0.373 0.392	0.394 0.415	0.376 0.405	0.356 0.391	0.436 0.410	0.406 0.385	0.422 0.391	0.670 0.536	0.645 0.500	0.555 0.465
ETTm2	96 0.164 0.249	0.189 0.277	0.201 0.291	0.197 0.286	0.198 0.288	0.214 0.288	0.205 0.273	0.211 0.274	0.260 0.335	0.199 0.274	0.197 0.271	
	192 0.222 0.288	0.241 0.315	0.258 0.334	0.250 0.322	0.235 0.312	0.284 0.332	0.275 0.316	0.281 0.318	0.289 0.350	0.261 0.322	0.254 0.314	
	336 0.275 0.323	0.286 0.348	0.324 0.373	0.337 0.375	0.293 0.348	0.331 0.362	0.329 0.350	0.341 0.355	0.324 0.369	0.326 0.366	0.313 0.353	
	720 0.361 0.378	0.375 0.402	0.488 0.464	0.480 0.461	0.427 0.428	0.402 0.408	0.437 0.411	0.485 0.428	0.394 0.409	0.455 0.439	0.416 0.415	
Avg.		0.256 0.310	0.273 0.336	0.317 0.365	0.316 0.361	0.288 0.344	0.307 0.347	0.311 0.337	0.329 0.343	0.316 0.365	0.310 0.350	0.295 0.338
Weather	96 0.141 0.184	0.171 0.225	0.160 0.214	0.159 0.213	0.157 0.211	0.198 0.222	0.220 0.217	0.199 0.211	0.243 0.255	0.203 0.238	0.194 0.235	
	192 0.184 0.227	0.221 0.271	0.210 0.260	0.215 0.266	0.208 0.256	0.247 0.265	0.271 0.259	0.246 0.251	0.278 0.329	0.256 0.290	0.249 0.285	
	336 0.235 0.268	0.274 0.311	0.274 0.309	0.291 0.322	0.255 0.290	0.283 0.303	0.286 0.297	0.274 0.291	0.306 0.346	0.314 0.336	0.302 0.327	
	720 0.303 0.318	0.356 0.370	0.418 0.405	0.415 0.400	0.405 0.397	0.373 0.354	0.373 0.354	0.337 0.340	0.350 0.374	0.397 0.396	0.372 0.378	
Avg.		0.216 0.249	0.256 0.294	0.265 0.297	0.270 0.300	0.256 0.288	0.275 0.286	0.287 0.281	0.264 0.273	0.294 0.326	0.292 0.315	0.279 0.306
ECL	96 0.125 0.218	0.141 0.237	— —	— —	— —	0.189 0.280	0.160 0.250	0.153 0.241	0.745 0.680	0.154 0.231	0.152 0.229	
	192 0.144 0.236	0.159 0.254	— —	— —	— —	0.205 0.292	0.175 0.263	0.169 0.255	0.755 0.683	0.179 0.254	0.172 0.250	
	336 0.161 0.256	0.177 0.272	— —	— —	— —	0.221 0.307	0.187 0.277	0.187 0.273	0.766 0.687	0.214 0.284	0.203 0.276	
	720 0.203 0.295	0.219 0.308	— —	— —	— —	0.258 0.335	0.228 0.309	0.237 0.313	0.794 0.696	0.311 0.346	0.289 0.337	
Avg.		0.158 0.251	0.174 0.278	— —	— —	— —	0.218 0.303	0.187 0.274	0.186 0.270	0.765 0.686	0.214 0.278	0.204 0.273
Average		0.282 0.329	0.305 0.351	0.348 0.381	0.352 0.380	0.337 0.370	0.338 0.360	0.328 0.346	0.341 0.349	0.515 0.481	0.410 0.387	0.396 0.379
1 st Count		51	3	1	0	3	0	2	5	1	0	0

* Dataset used for pre-training is not evaluated on corresponding models; dashes denote results (—).

* Traffic from PEMS (Liu et al., 2022a) is typically used for pre-training large time-series models and is therefore not evaluated here.

During our experiments, we did not use pre-trained versions of MoHETS, which is left for future work. To avoid visual disorder and save space for comparisons with a large set of baselines, we combined the main results of multiple experiments with different versions of MoHETS in Table 9 and Table 7 (see Section 4.1), presenting them as a single column. However, in Table 9, we detail the exact version of MoHETS and the training settings used to achieve the results presented in Table 9 and Table 7.

Table 9. Experiment configuration of MoHETS according to the main and additional results reported in Tables 1, 7, and 8. LR denotes learning rate.

Dataset	Model version	Training Process					
		P	H _o	LR	Min LR	Batch Size	Epochs
ETTh1	MoHETS _{tiny}	8	24	3.2×10^{-3}	1.2×10^{-4}	128	30
ETTh2	MoHETS _{tiny}	8	24	3.2×10^{-3}	1.2×10^{-4}	128	30
ETTm1	MoHETS _{base}	16	24	3.2×10^{-3}	1.2×10^{-4}	128	20
ETTm2	MoHETS _{base}	16	24	3.2×10^{-3}	1.2×10^{-4}	128	20
Weather	MoHETS _{large}	16	24	3.2×10^{-3}	1.2×10^{-4}	64	30
ECL	MoHETS _{large}	12	24	2.2×10^{-3}	1.2×10^{-4}	8	10
Traffic	MoHETS _{base}	12	24	2.2×10^{-3}	1.2×10^{-4}	6	15

B.1. Patch Lengths

Forecast performance can be sensitive to patch length P . Smaller values increase the sequence length (i.e., the number of patches), reducing computational efficiency and increasing GPU memory demands due to extended sequences. In contrast, larger values may overgeneralize local patterns, degrading accuracy in coarse-grained data. Previous works (Zhang & Yan, 2022; Nie et al., 2022; Wang et al., 2024b; Liu et al., 2024a) demonstrate the effects of different patch sizes, suggesting that moderate lengths (e.g., [8, 24]) offer a good balance between efficiency and capture of temporal patterns. We evaluate $P \in \{8, 12, 16\}$ (Nie et al., 2022), with Table 10 showing our best configurations according to each benchmark. As we can see, for coarse-grained hourly datasets, reduced patch lengths ($P \in \{8, 12\}$) yield superior performances, as they preserve local patterns critical for high-frequency signals. On the other hand, minute-level datasets benefit from longer patch lengths ($P = 16$), as larger patches capture broader temporal trends. Increasing or decreasing the length interval resulted in performance degradation, confirming that the optimal patch lengths depend on the dataset frequency (Zhang & Yan, 2022).

B.2. Output Horizons

We evaluate the trade-off between forecasting efficiency and accuracy, ablating MOHETS_{tiny} ($d_{\text{model}} = 64$ and $P = 8$) with different output horizons $H_o \in \{8, 16, 24, 32\}$ on ETTh1 and ETTh2, with MSE and MAE results averaged over the full horizons $H \in \{96, 192, 336, 720\}$. Table 10 presents the MSE, MAE, and total forecasting time for both datasets. Larger H_o values reduce the number of iterations (that is, $\lceil H/H_o \rceil$), enhancing the computational efficiency. For ETTh1, MSE improves from the output horizons $H_o = 8$ to $H_o = 24$ with a 7.0% reduction, before increasing with $H_o = 32$, indicating a possible overgeneralization. Similarly, the ETTh2 columns show a 12.1% reduction in MSE from $H_o = 8$ to $H_o = 24$. The forecast time decreases 69% from the output horizons $H_o = 8$ to $H_o = 24$, but the metrics degrade when H_o increases to 32. We observed similar behaviors for other benchmark datasets, which confirms $H_o = 24$ as an optimal balance between performance and precision.

Table 10. Ablation study with different output horizons. A lower MSE or MAE indicates a better prediction. The best results are in **bold**.

Dataset	ETTh1				ETTh2			
	Model version	P	H_o	MSE	MAE	MSE	MAE	Time (s)
MOHETS _{tiny}		8	8	0.412	0.430	0.396	0.408	113
		8	16	0.390	0.421	0.372	0.391	57
		8	24	0.383	0.412	0.348	0.382	35
		8	32	0.402	0.419	0.366	0.392	26

B.3. Scalability Analysis

Increasing model size and the number of training tokens generally improves performance, a phenomenon known as scaling laws (Kaplan et al., 2020). We evaluate the impacts of scalability on MoHETS's forecasting performance by varying the representation dimension $d_{\text{model}} \in \{64, 128, 256, 384\}$ (see Table 6). For these experiments, we use the ETTm1, ETTm2, Weather, and ECL datasets. ETTh1 and ETTh2 were excluded due to the high risks of overfitting on such small datasets (Nie et al., 2022), as well as Traffic, due to hardware constraints.

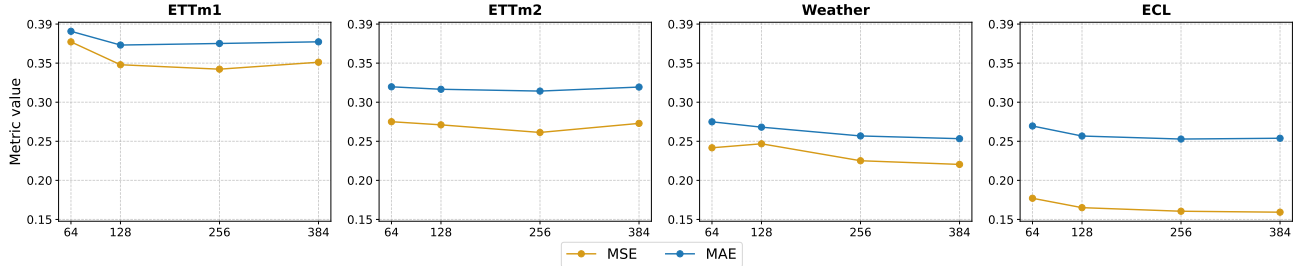


Figure 4. Scalability analysis on ETTm1, ETTm2, Weather, and ECL, with varying d_{model} sizes on the x-axis. Lower MSE or MAE indicates better performance.

Figure 4 shows that increasing the size of MoHETS improves both MSE and MAE, confirming scalability benefits in

the time-series domain (Shi et al., 2024). On ETTm1 and ETTm2, MSE decreases substantially up to $d_{\text{model}} = 256$, then increases slightly at $d_{\text{model}} = 384$, suggesting potential overfitting due to the limited data size. In contrast, MoHETS achieves consistent reductions in metrics up to $d_{\text{model}} = 384$ on Weather and ECL, indicating robust scaling benefits on larger datasets. These results not only align with scaling laws but also validate MoHETS’s potential for further scaling in resource-rich contexts.

C. Forecast Showcases

To provide a qualitative assessment of MoHETS’s performance, we visualize its forecasting results across different time dimensions from the test sets of the benchmark datasets, namely ETTh1, ETTh2, ETTm1, ETTm2, Weather, ECL, and Traffic (Figures 5 – 11). In each figure, the forecast horizon is set to 96 time steps. To enhance clarity and ensure intuitive visualizations, we display the full predicted horizon alongside a slice of the historical input data (look-back window) and the corresponding ground-truth future values.

These visualizations illustrate MoHETS’s ability to generate accurate and coherent forecasts in highly heterogeneous multivariate time series, underscoring the effectiveness of the proposed architecture. As demonstrated in quantitative evaluations (see Section B), MoHETS’s performance gains are particularly pronounced in long- and ultra-long-term prediction settings, where it robustly captures complex temporal dynamics. Overall, these qualitative results highlight the practical utility of MoHETS for state-of-the-art, long-term multivariate time series forecasting.

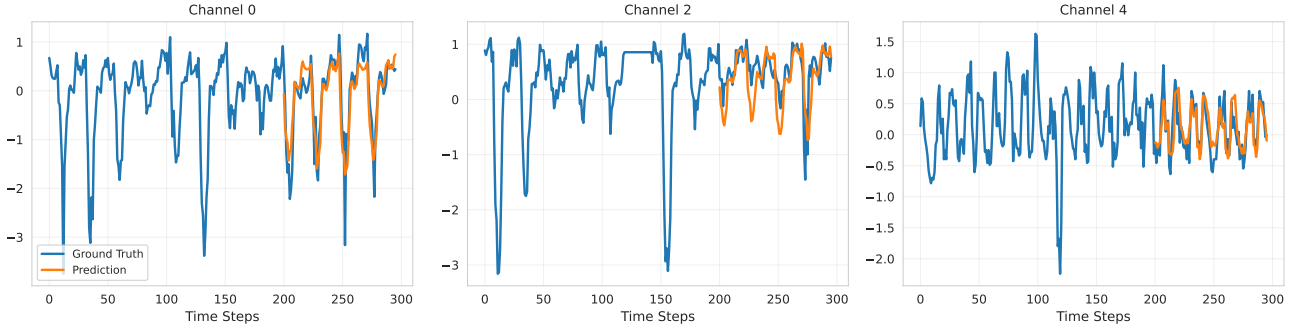


Figure 5. Forecast showcases of MoHETS across different time channels from ETTh1, with a horizon of 96. Blue curves are the ground truths, and orange curves are the model predictions. Curves before the model predictions are the input data.

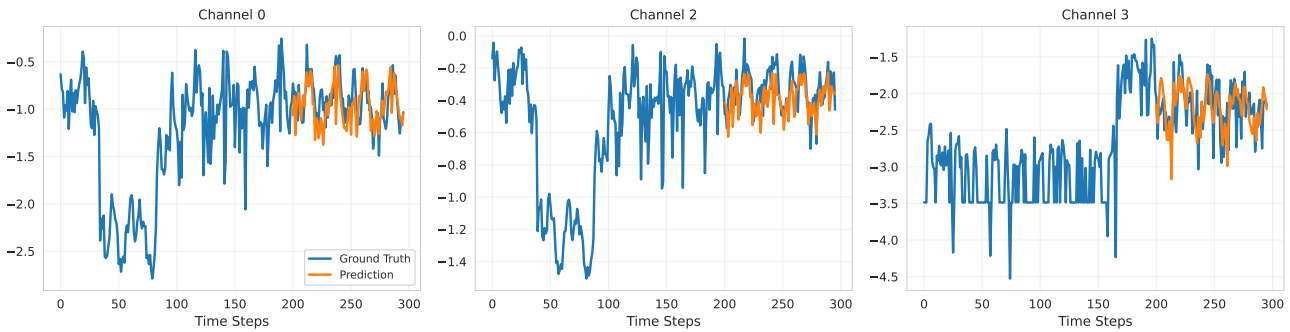


Figure 6. Forecast showcases of MoHETS across different time channels from ETTh2, with a horizon of 96. Blue curves are the ground truths, and orange curves are the model predictions. Curves before the model predictions are the input data.

D. Discussion, Limitations, and Future Work

Although both language and time series are sequential data with long-range dependencies, they differ fundamentally: language relies on deterministic structures and semantic patterns, whereas time series data often arise from stochastic processes with complex temporal dynamics. Time is not language. Consequently, effective temporal modeling requires

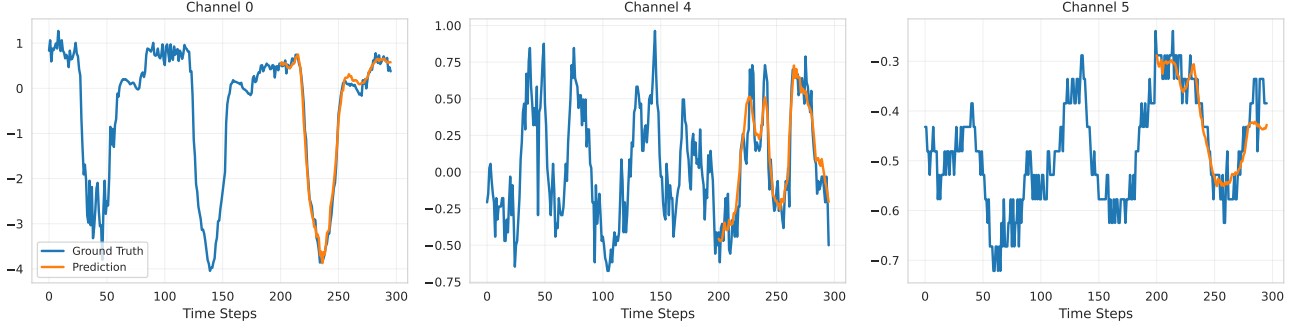


Figure 7. Forecast showcases of MoHETS across different time channels from **ETTm1**, with a horizon of 96. Blue curves are the ground truths, and orange curves are the model predictions. Curves before the model predictions are the input data.

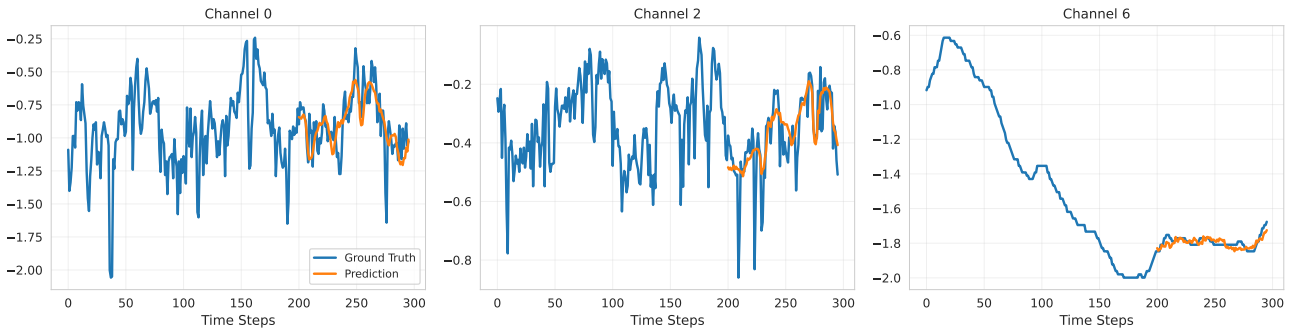


Figure 8. Forecast showcases of MoHETS across different time channels from **ETTm2**, with a horizon of 96. Blue curves are the ground truths, and orange curves are the model predictions. Curves before the model predictions are the input data.

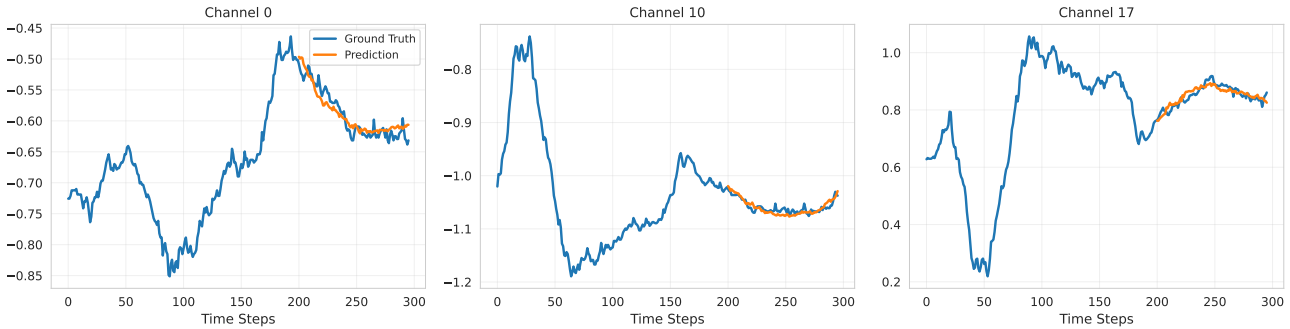


Figure 9. Forecast showcases of MoHETS across different time channels from **Weather**, with a horizon of 96. Blue curves are the ground truths, and orange curves are the model predictions. Curves before the model predictions are the input data.

specialized architectures beyond scaling language models. MoHETS introduces tailored innovations that combine multiple approaches, respecting temporal structures such as time continuity, seasonality, and non-stationarity.

Although MoHETS demonstrates significant capabilities, specific directions warrant further exploration. In contexts with large model configurations (e.g., $d_{\text{model}} = 384$) and high-dimensional datasets with numerous features, inference latency increases, particularly for ultra-long horizons (e.g., $H = 720$ time points). Increasing the output horizon significantly improves forecasting; however, long output horizons can degrade accuracy, especially on coarse-grained datasets, due to overgeneralization of temporal patterns. During our experiments, we identified $H_o = 24$ as an optimal balance between inference speed and precision on diverse benchmarks, outperforming standard “next-token” autoregressive predictions, because it allows us to generate $24 \times$ more future time points per iteration.

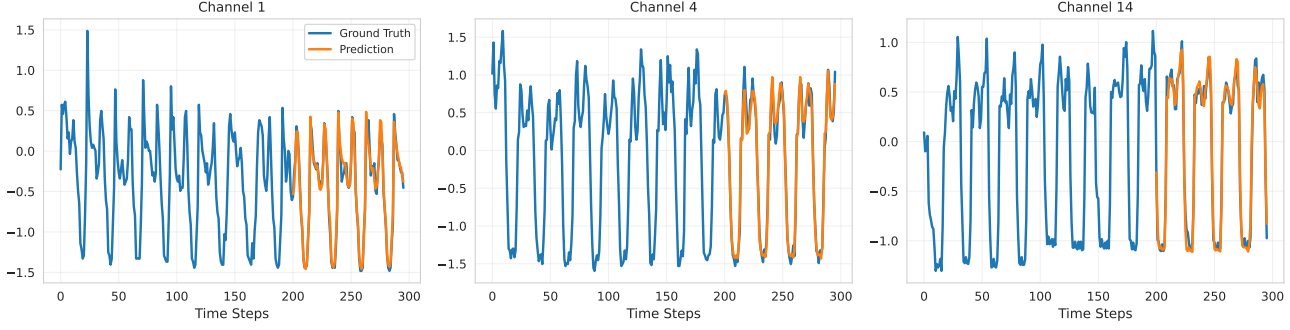


Figure 10. Forecast showcases of MoHETS across different time channels from **ECL**, with a horizon of 96. Blue curves are the ground truths, and orange curves are the model predictions. Curves before the model predictions are the input data.

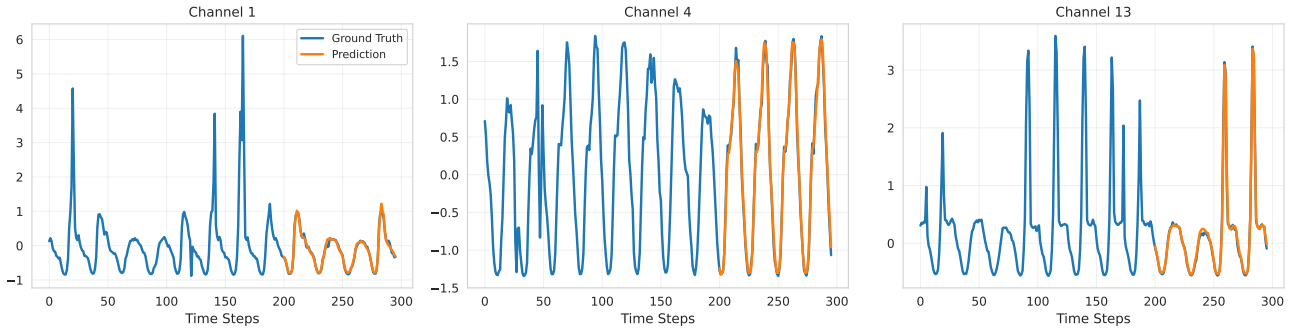


Figure 11. Forecast showcases of MoHETS across different time channels from **Traffic**, with a horizon of 96. Blue curves are the ground truths, and orange curves are the model predictions. Curves before the model predictions are the input data.

Caching mechanisms could be used to speed up forecasting. Widely used in language models to accelerate inference, KV Caching (Pope et al., 2023) has not been thoroughly investigated in time-series forecasting, particularly for patch-level attention encoders with multi-resolution outputs. Thus, adapting caching approaches to encoder-only models is a promising direction to reduce latency for long-horizon predictions. Another inspiring concept for future exploration is the multi-resolution projection head (Shi et al., 2024), in which multiple projection heads, each corresponding to a distinct forecasting horizon, are optimized during training to provide more flexibility for handling time-series data with different frequencies.

Enhancing covariate integration through adaptive mechanisms to handle missing or temporally misaligned exogenous covariates could improve robustness in real-world scenarios (Wang et al., 2024b). Furthermore, extending the Mixture-of-Heterogeneous-Experts (MoHE) to incorporate additional architectures (e.g., graph-based or attention-based experts) could capture more complex temporal dependencies, broadening MOHETS’s applicability to heterogeneous time-series tasks. Finally, scale and pre-train MOHETS on large-scale time-series datasets, such as Time-MoE (Shi et al., 2024) and TimesFM (Das et al., 2024), could enable zero-shot forecasting across diverse domains, leveraging the MoHE architecture’s sparsity for efficient large-scale training.